



## Hadronic Coupling Constants In Lattice Gauge Theory

STEVEN GOTTLIEB<sup>†</sup>  
University of California, San Diego  
La Jolla, CA 92093

PAUL B. MACKENZIE\*  
The Institute for Advanced Study  
Princeton, NJ 08540

H. B. THACKER  
Fermi National Accelerator Laboratory,  
P.O.Box 500, Batavia IL 60510

and

DON WEINGARTEN  
IBM, T. J. Watson Research Center,  
Yorktown Heights, N. Y. 10598

### ABSTRACT

We describe an efficient method for calculating hadronic three point functions in lattice gauge theory. We use the method to calculate the  $\pi$ -nucleon coupling constant and the coupling constants for the hadronic decays of the  $\rho$  and  $K^*$  mesons and the  $\Delta$ ,  $\Sigma^*$ , and  $\Xi^*$  baryons.

## I. INTRODUCTION

The valence [1] (quenched [2]) approximation to lattice QCD has been used so far in the calculation of hadron masses [1-3], magnetic moments [4], and weak operator matrix elements [5,6] and to study the nature of chiral symmetry breaking [7]. In the present article we will use this approximation to evaluate the coupling constants for  $\rho \rightarrow \pi\pi$ ,  $K^* \rightarrow K\pi$ ,  $N \rightarrow N\pi$ ,  $\Delta \rightarrow N\pi$ ,  $\Sigma^* \rightarrow \Sigma\pi$ ,  $\Sigma^* \rightarrow \Lambda\pi$  and  $\Xi^* \rightarrow \Xi\pi$ . Our preliminary results for some of these quantities were reported in ref. [8].

Although the predictions we obtain are qualitatively reasonable, we believe that our main result is actually not a specific set of numbers but rather a demonstration that the method we present is workable. The essence of our method is the addition of an external pion source to the action for the quarks. Three point functions are then obtained by differentiating two point functions with respect to the external source. Thus our three point function calculations are not much more difficult than the standard two point function calculations [1-3] which have been used to obtain hadron masses. An extension of this method might eventually be used to evaluate higher n-point functions to obtain scattering amplitudes.

We will begin, in Sect. II, by briefly defining our notation for the path integral expression for vacuum expectation values in lattice QCD. In Sect. III we will review the procedure for extracting hadron masses from two-point functions, and coupling constants from three-point functions. In Sect. IV we will discuss how we obtain three-point functions from two-point functions evaluated in an external field. In Sect. V we will present results for hadron masses obtained as a

by-product of the coupling constant calculations, and in Sect. VI we will describe the coupling constant evaluation itself. Sect. VII contains some concluding remarks. In the Appendix we present a new and much improved method for statistical analysis of physical quantities.

## II. PATH INTEGRAL

The theory is defined on a four-dimensional hypercubic periodic lattice with lattice spacing  $a$  and periodicity  $N_\mu$  in the  $\mu$  direction. On each nearest neighbor lattice link  $(x,y)$  is defined a variable  $U(x,y) \in SU(3)$ . On each lattice site are defined the Grassman variables  $\psi_{sc}^f(x)$ ,  $\bar{\psi}_{sc}^f(x)$ , where  $f$  is a flavor index,  $s$  is a spin index running from 1 to 4 and  $c$  is a color index running from 1 to 3. Let the gauge action  $S_G$  be the usual sum over plaquette contributions multiplied by  $g_0^{-2}$  for bare gauge coupling constant  $g_0$ . Define the quark action  $S_Q$  to be  $\sum \bar{\psi}(x) C_{xy} \psi(y)$  where the coupling matrix  $C_{xy}$  is -1 for  $x$  equal to  $y$  and  $K(r\bar{\gamma}_\mu)U(x,y)$  for  $y$  displaced from  $x$  by one link in the  $\pm\mu$  direction. The hopping parameter  $K$  is  $(8r+2m_0a)^{-1}$ , where  $m_0$  is the bare quark mass and  $r$  is the chirality parameter.

The vacuum expectation value of a product of quark fields and a function  $F$  of the link variables is

$$\langle F \prod \psi(u_i) \bar{\psi}(v_i) \rangle = Z^{-1} \int d\mu \int dv F \prod \psi(u_i) \bar{\psi}(v_i) \exp(S_G + S_Q), \quad (2.1)$$

where  $u_i$  and  $v_i$  are multi-indices combining position, flavor, spin and color,  $d\mu$  is a product of one copy of Haar measure on each independent link variable,  $dv$  is a Grassman integral over the quark fields, and  $Z$  is defined by the condition  $\langle 1 \rangle = 1$ . If quark fields are integrated out of the path integral and the valence approximation is introduced, the vacuum expectation becomes

$$\langle F \prod \bar{\psi}(u) \psi(v) \rangle = Z^{-1} \int d\mu F \det_{ij} |C_{u_i v_j}^{-1}| \exp(S_G) . \quad (2.2)$$

For any choice of  $u_i$  and  $v_j$  eq. (2.2) can be evaluated numerically [1-8] by the combination of a Monte Carlo algorithm [9] to perform the integral over link fields and a Gauss-Seidel iteration [10] to determine the matrix elements of  $C^{-1}$  needed for each Monte Carlo link configuration.

### III MASSES AND COUPLING CONSTANTS FROM CORRELATION FUNCTIONS

In this section we will review the relation between hadron masses and lattice two-point functions. Then we will consider how coupling constants can be extracted from three-point functions.

To evaluate masses and coupling constants we need a collection of field operators. For a pseudoscalar  $s$  or vector particle  $v$  define the field operators

$$s(x) = \bar{\psi}^f(x) \gamma^5 \psi^g(x) \phi_s^{fg} , \quad (3.1)$$

$$v_\mu(x) = \bar{\psi}^f(x) \gamma_\mu \psi^g(x) \phi_v^{fg} .$$

For a baryon  $B$  or antibaryon  $\bar{B}$  define the fields

$$B(x) = \psi_{ia}^f(x) \psi_{jb}^g(x) \psi_{kc}^h(x) \epsilon^{abc} \chi_B^{ijk} \phi_B^{fgh} , \quad (3.2)$$

$$\bar{B}(x) = \bar{\psi}_{ia}^f(x) \bar{\psi}_{jb}^g(x) \bar{\psi}_{kc}^h(x) \epsilon^{abc} \chi_B^{ijk} \phi_B^{fgh} .$$

The quantities  $\phi^{fg}$  and  $\phi^{fgh}$  in eqs. (3.1) and (3.2) are flavor wave functions,  $\chi^{ijk}$  in eq. (3.2) is a spin wave function, and  $\epsilon^{abc}$  in eq. (3.2) is the alternating index. The flavor wave functions are normalized in such a way that the only nonvanishing entries for  $\pi^+$ ,  $\rho^+$ , proton, antiproton,  $\Delta^{++}$  and  $\bar{\Delta}^{--}$  are

$$\begin{aligned}
\phi_{\pi^+}^{du} &= \phi_{\rho^+}^{du} = 1, \\
\phi_p^{uud} &= \phi_{\bar{p}}^{uud} = 1, \\
\phi_{\Delta^{++}}^{uuu} &= \phi_{\bar{\Delta}^{--}}^{uuu} = 1.
\end{aligned} \tag{3.3}$$

The spin wave functions in (3.2) are normalized so that for a proton or antiproton with  $s_z$  of 1/2 and a  $\Delta^{++}$  or  $\bar{\Delta}$  with  $s_z$  of 3/2 the only nonzero components are

$$\begin{aligned}
\chi_p^{112} &= -\chi_p^{121} = 1, \\
\chi_{\bar{p}}^{443} &= -\chi_{\bar{p}}^{434} = 1, \\
\chi_{\Delta}^{111} &= 1, \\
\chi_{\bar{\Delta}}^{444} &= 1.
\end{aligned} \tag{3.4}$$

Now let  $A(x)$  be one of the fields defined in eqs. (3.1) and (3.2). Define  $\tilde{A}(\vec{q};t)$  to be the Fourier transformed field

$$\tilde{A}(\vec{q};t) = \sum_{\vec{x}} \exp(i \vec{q} \cdot \vec{x}) A(\vec{x}, t). \tag{3.5}$$

Then for large values of  $t$  and of the 4-direction lattice periodicity  $N_4$  with  $t \ll N_4$  the correlation function of the adjoint operator  $\tilde{A}^\dagger(\vec{q};t)$  and  $A(0)$  has the asymptotic behavior

$$\langle A^\dagger(0)\tilde{A}(\vec{q};t) \rangle \rightarrow Z_A(\vec{q})\exp[-E_A(\vec{q})t] \quad , \quad (3.6)$$

where  $E_A(\vec{q})$  is the energy in lattice units of the least energetic state  $|A,\vec{q}\rangle$  with momentum  $\vec{q}$  which  $A(0)$  can create from the vacuum. The coefficient  $Z_A(\vec{q})$  in eq. (3.6) is given by

$$Z_A(\vec{q}) = (N_1 N_2 N_3)^{-1} |\langle A,\vec{q}|\tilde{A}(\vec{q};0)|\Omega\rangle|^2 \quad , \quad (3.7)$$

where  $|\Omega\rangle$  is the vacuum state. Both  $|\Omega\rangle$  and  $|A,\vec{q}\rangle$  are normalized to one in this expression. A proof of eq. (3.6) can be obtained by representing the expectation value as the trace of a product of Heisenberg field operators and then inserting a complete set of Hamiltonian eigenstates between the pair of field operators. The masses reported in, for example, ref. [1-3] were obtained by fitting Monte Carlo values of the expectation on the left side of eq. (3.6) to the asymptotic form on the right side with  $\vec{q}$  set equal to zero.

In the valence approximation, which includes contributions of the form shown in Fig. 1a but omits virtual fermion loops such as Fig. 1b, resonances such as the  $\rho$  do not couple to decay channels. As a result the energies which appear in eq. (3.6) for each resonance field will be the energies of the corresponding resonance. Thus the energy variable in eq. (3.6) for the field  $\rho_\mu(x)$  will be the energy of a  $\rho$  with momentum  $\vec{q}$ . In the full theory including fermion loops, however, if the volume of space is made sufficiently large and the masses of quarks sufficiently small, strong resonances will be able to decay. The energy entering eq. (3.6) for a resonance field will be the energy of the decay products. For  $\rho_\mu(x)$  this will be the energy of a  $2\pi$  state. If the

volume of space is small or the masses of quarks large, on the other hand, the theory including fermion loops will have the same behavior as the valence approximation. For the case of small spatial volume, this is because the decays of the lightest vector and baryon resonances occur only to states with orbital angular momentum of one. Therefore, the minimum energy for decay states with nonzero orbital angular momentum will be above the masses of the resonances. If the quarks are heavy, the mass of the decay products will be pushed above the resonance mass. As a result, the resonances will become stable.

Let us now consider expectation values of products of three fields and the relation of these quantities to hadron coupling constants. For large values of  $t_1$  and  $t_2$  with  $N_4 \gg t_2 \gg t_1$ ,

$$\langle \tilde{A}(0;t_2) \tilde{\pi}(\vec{q};t_1) B(0) \rangle \rightarrow Z_{AB\pi}(\vec{q}) \exp[-E_A(0)(t_2-t_1) - E_B(\vec{q})t_1]. \quad (3.8)$$

Here  $E_A(0)$  and  $E_B(\vec{q})$  are, respectively, the energy in lattice units of the lightest rest state created from the vacuum by  $A^\dagger(0)$ , and the energy of the lightest state with momentum  $\vec{q}$  created from the vacuum by  $B(0)$ . Eq. (3.8) can be proved by nearly the same argument which yields eq. (3.6). The coefficient  $Z_{AB\pi}(\vec{q})$  in (3.8) becomes

$$Z_{AB\pi}(\vec{q}) = [Z_A(0)Z_B(\vec{q})]^{1/2} \langle A, 0 | \tilde{\pi}(\vec{q}; 0) | B, \vec{q} \rangle. \quad (3.9)$$

In both the valence approximation and the full theory including fermion loops, it is possible for the field  $\tilde{A}(0;t_2)$  in eq. (3.8) to couple the vacuum to a  $B\pi$  state. As was the case for propagators, however, if quark mass is sufficiently large or the volume of space sufficiently

small the lightest state which  $\tilde{A}(0;t_2)$  creates from the vacuum will still consist of a single A particle. This situation holds for the numerical results we will present in sect. 6 and will be assumed for the remainder of the present discussion.

According to the LSZ reduction formula,  $\langle A, 0 | \tilde{\pi}(\vec{q}; 0) | B, \vec{q} \rangle$  is equal to the  $A \rightarrow B\pi$  three point function truncated by removing appropriately normalized free propagators on the A and B legs of the vertex. What remains is a free propagator for the  $\pi$  leg, a kinematic factor for the truncated vertex, and the  $A \rightarrow B\pi$  coupling constant. Define the free field lattice propagator

$$P(E, \omega) = \sum_{t=-\infty}^{\infty} e^{Et} e^{-\omega|t|} \tag{3.10}$$

$$= \frac{\sinh \omega}{\cosh \omega - \cosh E}$$

Then we have

$$\langle B, \vec{q} | \tilde{\pi}(\vec{q}; 0) | A, 0 \rangle =$$

$$g_{AB\pi} K(\vec{q}) \sqrt{\frac{Z_{\pi}(\vec{q})}{2E_B(q)2E_A(0)2E_{\pi}(q)}} P[E_A(0) - E_B(\vec{q}), E_{\pi}(\vec{q})] \tag{3.11}$$

Assembling eq. (3.8)-(3.11) we obtain for large  $t_1$  and  $t_2$  with  $N_4 \gg t_2 > t_1$

$$\langle \tilde{A}(0; t_2) \tilde{\pi}(\vec{q}; t_1) B(0) \rangle \rightarrow \sqrt{\frac{Z_A(0) Z_B(\vec{q}) Z_\pi(\vec{q})}{2E_A(0) 2E_B(\vec{q}) 2E_\pi(\vec{q})}} K(\vec{q}) \quad (3.12)$$

$$\times g_{AB\pi} \sum_{t=-\infty}^{\infty} \exp[-E_A(0)|t_2-t|] \exp[-E_\pi(\vec{q})|t_1-t|] \exp[-E_B(\vec{q})|t|] .$$

A normalization convention for the kinematic factor  $K(\vec{q})$ , and thus for the coupling constant  $g_{AB\pi}$ , in eqs. (3.11) and (3.12) can be chosen conveniently by requiring truncated on shell three point functions to be given by a specified effective interaction in the continuum limit. For the coupling of a vector  $v$  to a pseudoscalar  $s$  and a  $\pi$  the most general effective vertex can be cast in the form

$$S_{\text{eff}} = g_{v s \pi} \int d^4x v_\mu^i(x) s^j(x) \partial_\mu \pi^k(x) \Gamma^{ijk} \quad (3.13)$$

where  $\Gamma^{ijk}$  is a Clebsch-Gordon coefficient for the coupling among the isospin indices  $i, j$ , and  $k$ . Our normalization of  $\Gamma^{ijk}$  is chosen so that for the vertices  $\rho^+ \rightarrow \pi^+ \pi^0$  or  $K^{*+} \rightarrow K^+ \pi^0$  we have

$$K(\vec{q}) = 2|\vec{q}|. \quad (3.14)$$

Here the initial vector particle is assumed at rest with spin component 0 along the direction of  $\vec{q}$ .

For the coupling between nucleons and a pion,  $N \rightarrow N\pi$ , the most general effective vertex is

$$S_{\text{eff}} = g_{NN\pi} \int d^4x \bar{N}(x) \gamma^5 \tau^i N(x) \pi^i(x) \quad , \quad (3.15)$$

where  $\tau^i$  is a Pauli spin matrix acting on the nucleon isospin indices. For  $p \rightarrow p\pi^0$  with equal spin components of initial and final proton along direction  $\vec{q}$ ,

$$K(\vec{q}) = |\vec{q}| \sqrt{\frac{2m_N}{E_N(\vec{q}) + m_N}} \quad . \quad (3.16)$$

For the coupling between a spin 3/2 baryon  $B^*$ , a spin 1/2 baryon  $B$  and a pion the most general effective vertex is

$$S_{\text{eff}} = \frac{g_{B^*B\pi}}{\sqrt{m_{B^*}m_B}} \int d^4x B_\mu^{*i}(x) B^j(x) \partial_\mu \pi^k(x) \Gamma^{ijk} \quad , \quad (3.17)$$

where  $\Gamma^{ijk}$  is again a Clebsch-Gordon coefficient on the isospin indices  $i, j$  and  $k$ . Our normalization of  $\Gamma^{ijk}$  is chosen so that for the decays  $\Delta^+ \rightarrow p\pi^0$ ,  $\Sigma^{*+} \rightarrow \Sigma^+\pi^0$ ,  $\Sigma^{*0} \rightarrow \Lambda\pi^0$  and  $\Xi^{*0} \rightarrow \Xi^0\pi^0$  with equal initial and final baryon spin components along  $\vec{q}$

$$K(\vec{q}) = 2|\vec{q}| \sqrt{\frac{E_B(\vec{q}) + m_B}{2m_B}} \quad . \quad (3.18)$$

This means that our coupling constants are appropriate to the given partial width rather than to the full width.

The coupling constants and kinematic factors which we have defined are simply related to decay widths in the infinite volume continuum theory. By taking the absolute square of these amplitudes, averaging

over initial spin states, summing over final spin state and two-body phase space we obtain the width

$$\Gamma(A \rightarrow B\pi) = \frac{|\vec{q}| K^2(\vec{q}) g_{AB\pi}^2}{d(2J_A + 1) \pi m_A^2}, \quad (3.19)$$

where  $d$  is 8 for meson decays and 4 for baryon decays.

## IV CORRELATION FUNCTIONS IN AN EXTERNAL FIELD

For calculating hadron propagators, Fourier transforming one of the two operators by summing over an entire time slice achieves a useful increase in statistics for negligible additional computer time and in addition makes the propagators easier to analyze by removing power factors, leaving simple exponentials. Similarly, for the three-point functions, we would like two of the three operators to be Fourier transformed to achieve both a gain in statistics and a simple convolution of exponentials in the functional form to be fit. In practice, however, the direct calculation of Fourier transformed three-point functions from products of quark propagators cannot be carried out in a reasonable amount of computer time. To calculate directly values of a three-point function at all the points needed to form the Fourier transforms of the pion field and the A field in eq. (3.12) would require running a Gauss-Seidel iteration  $O(N_1 N_2 N_3)$  times on each Monte Carlo gauge configuration. This would cost far too much computer time. An alternative procedure is to obtain the three-point function of (3.12) by differentiating the AB two-point function with respect to an external pion field. The expectation value we need can be written

$$\langle \tilde{A}(0; t_2) \tilde{\pi}(\vec{q}; t_1) B(0) \rangle = \frac{\partial}{\partial \alpha} \langle \tilde{A}(0; t_2) B(0) \rangle_{\alpha} \Big|_{\alpha=0} \quad (1)$$

where  $\langle \dots \rangle_{\alpha}$  is a vacuum expectation with quark action  $S_Q$  in eq. (2.2) modified by adding an external pion source

$$\begin{aligned}
S'_Q &= S_Q + \frac{\alpha}{2i} [\tilde{\pi}^0(\vec{q}; t_1) - \tilde{\pi}^0(-\vec{q}; t_1)] \\
&= \sum_{xy} \bar{\psi}(x) C_{xy} \psi(y) + \alpha \sum_{xy} \bar{\psi}(x) D_{xy} \psi(y) .
\end{aligned} \tag{4.2}$$

In this equation  $\tilde{\pi}^0(\vec{q}, t_1)$  is a Fourier transformed  $\pi^0$  field defined by eqs. (3.1), (3.3) and (3.5). The effect of the  $\pi^0$  terms in (4.2) on the valence approximation path integral is to replace eq. (2.2) with

$$\langle F \prod \psi(u_i) \bar{\psi}(v_i) \rangle_\alpha = Z^{-1} \int d_\mu F \det_{ij} |(C + \alpha D)_{u_i v_j}^{-1}| \exp(S_G) . \tag{4.3}$$

The procedure we adopt to measure  $\langle \tilde{A}(0; t_2) \tilde{\pi}(\vec{q}; t_1) B(0) \rangle$  is to evaluate  $\langle \tilde{A}(0; t_2) B(0) \rangle_\alpha$  from eq. (4.3) using Monte Carlo and Gauss-Seidel and then differentiate with respect to  $\alpha$ . The amount of work required to find  $\langle \tilde{A}(0; t_2) B(0) \rangle_\alpha$  by Monte Carlo and Gauss-Seidel is no greater than what is needed for an ordinary two-point function. In particular we need only  $O(1)$  Gauss-Seidels for each Monte Carlo gauge configuration, not  $O(N_1 N_2 N_3)$ .

It was not self-evident when we began our calculation that we actually would be able to find reliable values of the derivative of Monte Carlo averages with respect to a parameter. We found that this could be done, however, if a single ensemble of gauge configurations is used to evaluate the averages for a number of different choices of  $\alpha$ . If different ensembles of gauge configurations are used at each different  $\alpha$ , statistical fluctuation occur in  $\langle \tilde{A}(0; t_2) B(0) \rangle_\alpha$  from one  $\alpha$  to the next and differentiation becomes difficult. On the other hand, using the same gauge configurations we found that for small values of  $\alpha$

( $\leq 0.05$ ) the dependence on  $\alpha$  is linear to within about 1% and the derivative can be measured quite accurately. Our final numbers were obtained by taking the difference between results at  $\alpha$  of 0.0 and 0.025.

## V. HADRON SPECTROSCOPY

## A. General Remarks

To perform the analysis for the coupling constants, it was necessary to carry out a complete mass analysis for the relevant hadrons. We report on that analysis separately in this section. Using the operators defined in Sec. III, we may determine the asymptotic form of two point functions for mesons and baryons. For mesons, including a term for the backward propagating signal resulting from periodic boundary conditions, we have

$$\langle m(0)\tilde{m}(\vec{q};t) \rangle \rightarrow Z_m (e^{-E(q)t} + e^{-E(q)(N_4-t)}) \quad (5.1)$$

for  $t$  and  $(N_4-t)$  sufficiently large, where  $N_4$  is the lattice periodicity in the time direction. As is well known, it is very costly in computing of time make  $N_4$  too long, so there is a significant contribution to the meson two point function from higher energy states at moderate values of  $t$  and  $N_4-t$ . One may attempt to deal with this complication by fitting meson propagators to a form which includes the contribution of two states

$$\begin{aligned} \langle m(0)\tilde{m}(\vec{q};t) \rangle = & Z_l (e^{-E_l(q)t} + e^{-E_l(q)(N_4-t)}) + \\ & Z_h (e^{-E_h(q)t} + e^{-E_h(q)(N_4-t)}) \end{aligned} \quad (5.2)$$

with the parameters  $Z_l$  and  $E_l$  referring to the light particle and  $Z_h$  and  $E_h$  referring, to the heavy particle. This procedure suffers from the problems of fitting a small set of data with a large number of

parameters.

The fitting of the propagator may be carried out in a second way. From (5.1) we may determine an effective energy as a function of  $t$  by taking the ratio of the two point function for successive  $t$  values

$$\frac{\langle m(0)\tilde{m}(\vec{q};t) \rangle}{\langle m(0)\tilde{m}(\vec{q};t+1) \rangle} = \frac{e^{+E_q}(1+e^{-E_q(N_4-2t)})}{1+e^{-E_q(N_4-2t-2)}} \quad (5.3)$$

This may be solved for the effective energy  $E_q$ , as a function of  $t$ . One nice feature of plotting the effective energy as a function of  $t$  is that it provides a test of whether  $N_t$  is large enough. It is necessary that the effective energy curve go to a constant in order to conclude that one has separated the lowest energy state from excitations.

Generally, the two point functions are not fit well with Eq. (5.2) for  $t$  very small. The heavy particle parameters vary a great deal when the number of small  $t$  points used in the fitting is varied; however, the variation of the light parameters is small, and can be used to estimate the systematic error. The operators we have defined for the baryons use upper component quark fields only and therefore have asymmetric behavior forward and backward in time. We limit our study of the baryon propagators to the signal propagating forward in time. Since the signal propagating backward in time is small for the baryons, this amounts to restricting  $t$  to be less than about half way across the lattice in the time direction. We fit the baryon two point function to a form which includes the contribution of two states.

$$\langle b^\dagger(0)\tilde{b}(\vec{q};t)\rangle = z_l e^{-E_l(q)t} + z_h e^{-E_h(q)t} \quad (5.4)$$

for  $t \lesssim N_4/2$ . As with the mesons, we can determine the energy in a second way. The effective energy formula for baryons is

$$E_q(t) = \ln \left( \frac{\langle b^\dagger(0)\tilde{b}(\vec{q};t)\rangle}{\langle b^\dagger(0)\tilde{b}(\vec{q};t+1)\rangle} \right) . \quad (5.5)$$

The remarks with regard to self consistency and systematic errors made in the case of meson spectroscopy also apply to baryons.

Our calculations are done on a lattice  $6^2 \times 12 \times 18$  with 12 taken as the 3-direction (decay axis) and 18 as the 4-direction (time). The large transverse size of the lattice is required to make possible sufficiently small values of pion momenta to place the external pion close to mass shell. The decays we consider produce final states with orbital angular momentum 1 and therefore vanish if the final pion is given a momentum of exactly zero. With a transverse size of 12 the minimum nonzero momentum for our choice of parameters is about 500 MeV compared to the physical decay momenta of 150-350 MeV for the processes we consider. We use  $\beta$  of 5.7, the same value chosen in ref. [1]. Gauge configurations were generated using the Metropolis algorithm. After equilibrating 1000 Monte Carlo sweeps, a gauge configuration was saved after each 500 sweeps. An ensemble of 20 gauge configurations was analyzed. For each configuration, quark propagators were computed for three mass values corresponding to  $K$  of 0.325, 0.340 and 0.355. We used a chirality parameter  $r$  of 0.5 for reasons discussed in ref. [1]

## B. Meson Spectroscopy

Two point functions for the pion and rho have been calculated using a variety of operators at the movable end of the two point function. Non-local operators for the pion were also considered as an alternative source of pions. The Gauss-Seidel inversion technique provides the quark propagator from a fixed source site to all other sites on the lattice, thus one can easily calculate

$$\langle \bar{\psi}(0) \gamma^5 \psi(0) \bar{\psi}(x) \gamma^5 U(x,y) \psi(y) \rangle$$

where  $U$  is a product of gauge matrices. We have considered operators where  $y = x + \hat{\mu}$ ,  $x + 2\hat{\mu}$ ,  $x + \hat{\mu} + \hat{\nu}$ ,  $x + 3\hat{\mu}$ , that is, operators where the quark and antiquark are separated by 1, 2,  $\sqrt{2}$ , and 3 lattice units respectively. In all cases we sum over spatial directions to get a rotationally invariant operator. Similar operators were considered for the rho. All operators yielded similar mass estimates, giving confidence in the reliability of the results. This would likely not have held true for the baryons, had we tested similar operators for them, since there is little reason to believe our baryon propagators to have reached their asymptotic behavior (see below).

In Figures 2 and 3 we show the two point functions for the local pion and rho. Figure 4 contains plots of the effective meson mass as a function of  $t$ . We see that even with a lattice size of eighteen in the time direction the lattice is not as long as one would like. There is a decrease in the slope of  $m(t)$ , but no flat region. For large  $t$ , the slope for the pion is smaller than that for the rho. The propagators were also fit according to Eq. (5.2). Typical fits are shown in Figures 2 and 3. The contribution from the light state is shown separately.

Because the process we are interested in involves pions with non-zero momentum, we have also measured the two point function for particles with momentum. The particle energy is in good agreement with relativistic dispersion. The normalization factor  $Z_1$  does not have the expected form  $\text{constant}/E_1$ ; however, a small error in mass is correlated with a large error in  $Z_1$ .

### C. Baryon Spectroscopy

We have looked at two point functions for the  $N$ ,  $\Delta$ ,  $\Lambda$ ,  $\Sigma$ ,  $\Sigma^*$ ,  $\Xi$ ,  $\Xi^*$ , and the  $\Omega^-$ . The up and down quark masses are taken to be equal. In Figure 5 and 6 we show the two point functions for the delta and nucleon up to half way across the lattice. The propagator remains positive for one more plane, before going negative because of the periodic boundary conditions. The last positive point is seen to deviate significantly from a good straight line fit to the propagator for  $t=7,8,9$ , especially for lighter quark masses. In Figure 7 we show the effective mass as a function of the distance from the source. For both the nucleon and the  $\Delta$ , there is clearly no region of flat behavior of a pure state before the signal propagating the "wrong" way around the lattice becomes important at time slice 9. In order to get more insight into the errors and finite time effects, we show in figures 8 and 9 effective mass plots for separate baryon spin states analyzed individually. We note that they are by no means degenerate, as they should be. The plots are shown for the lightest of our three quark mass values, which gave the largest spread among spin states.

In the case of the nucleon, we also split the data up into four groups by averaging all states together in ensembles of five lattices as shown in Figure 10. Here the spread of the effective mass increases as one goes from  $t=6$  to  $t=8$ . One sees that the spread between ensembles is bigger than the spread of different states.

#### D. Extrapolation in the hopping parameter and discussion of errors

It is well known that the Gauss-Seidel technique fails to converge for small quark mass. Thus, it is necessary to do an extrapolation to the physical value for the up and down quark masses. In Figure 11, we put  $m_\pi^2$  and  $m_p$  versus  $1/2K$ . From the x axis intercept of the pion line, we determine the critical value,  $K_c$ , where the pion mass vanishes. This is approximately the physical value since the pion is so light. Mass ratios may be computed without a knowledge of the lattice spacing  $a$ . The hopping parameter for the strange quark may be determined in a number of ways. We choose to fix the ratio of a strange hadron mass to a non-strange hadron mass. In particular, we have picked  $\Omega^-$  and  $\Delta$ , since this choice causes all baryon masses to agree well with experiment. An alternative would be to use the string tension to fix the scale and a strange particle mass, to fix the strange quark mass.

Table I shows how the particle masses change when the fitting procedure used to determine a mass from the propagator is varied. The first column (DE) corresponds to a fit including the contribution of two exponentials (see Eqs. (5.2) and (5.4)), ignoring the first three points of the propagator in the fit. Subsequent columns come from using the effective mass (see Eqs. (5.3) (5.5)), with distances 6,7, and 8 (EM6,7, and 8). We note that the masses fall as the distance increases

in accord with figures 4 and 7. The masses in the upper half of Table I are given in units of inverse lattice spacing. Much of the variation in the values for different fitting procedures corresponds merely to an overall change of scale. We have therefore also shown the masses scaled to the calculated nucleon mass. One sees that the strange particle masses vary less than 10 percent, and the delta by less than 10 percent.

The statistical errors were estimated using the jackknife method, which we describe separately in the Appendix. The essence of the method is to obtain the estimated error from the variance of the results obtained by analyzing data sets with one (or a few) elements removed from the original data set. This is a much more stable and reliable procedure than the usual method of analyzing subensembles containing a relatively small number of lattices. Subensembling is possible in this approach by removing increasingly large sets of consecutive lattices. A subensembling analysis for our hadron masses yielded identical error estimates (to within 5 or 10%) when 1, 2, or 4 consecutive lattices were removed, indicating no serious correlations. Since our lattices are separated by 500 Monte Carlo sweeps (thought to be a large number) this is not surprising. (However, more surprisingly, for our coupling constants we found small but noticeable correlations over 1000-1500 sweeps; see below.) Our calculated masses with statistical errors are compared with experiment in Table II.

#### E. Comparison With Other Calculations

It is easiest to make a comparison with other groups whose calculations are most similar to ours. Duffy et al <sup>11</sup> have done a calculation on a  $6^3 \times 14$  lattice with  $\beta=5.7$ . Since we both use the same

values of the hopping parameter a direct comparison may be made. Our pion masses are slightly lower, with  $1/2K_c$  given by 1.29 in our case and 1.25 in theirs. The rho masses are roughly comparable. Our nucleon and delta masses are quite a bit lower. Of course, we have seen that the effective mass is dropping as  $t$  increases. It is therefore not surprising that our lattice, which is longer in  $t$  than that of Ref. 11, gives lower baryon masses. Comparing  $m_{\text{eff}}(6)$  with the results plotted in Ref. 11, our delta is somewhat heavier, our nucleon somewhat lighter. When the extrapolation is made to the physical quark mass, our rho to proton ratio is .60, compared to the value .44 in Ref. 11. The physical value is .82. For the delta to nucleon ratio, our result is 1.32 compared to 1.04 for Ref. 11 and 1.31 for experiment. There is some improvement on our larger lattice.

Bowler et al<sup>12</sup> have recently reported a study on an  $8^3 \times 16$  lattice at  $\beta = 5.7$ . They have used Neumann boundary conditions in time. If one looks at their effective mass plots, it appears that the mass is no longer dropping by what in our notation is  $m_{\text{eff}}(6)$  ( $m_{\text{eff}}(10)$  in their notation). With periodic boundary conditions the masses are still falling. Since we have the same coupling, and these authors report their masses in lattice units, it is easy to compare results. The rho mass agrees within errors. Our nucleon mass is 1 to 1.5 standard deviations lower in lattice units. Our delta is 1.5 to 2 standard deviations heavier. It is not clear what accounts for the difference in the delta-proton mass difference. The total volumes of the lattices are comparable since the sizes are  $6^2 \times 12$  and  $8^3$ . There could be a slope dependence, or the fact that we used different operators for the baryons could play a role. There have been a number of calculations at  $\beta=6$  with

a comparable or smaller spatial lattice size. The physical box size is smaller because the coupling is weaker. Lipps et al.<sup>12</sup> have done a calculation on a  $10^3 \times 20$  lattice. They found an improvement in  $m_\rho/m_p$ . Their value was .66. The delta proton splitting was a bit smaller.

## VI. HADRON COUPLING CONSTANTS

To obtain coupling constants from the three point function data, energy and renormalization constant parameters obtained from the previously described two point function analysis are plugged into the expected functional form of the three point function, eq. (3.12). The remaining parameter in (3.12),  $g_{AB\pi}$ , is then obtained by comparing (3.12) with the Monte Carlo data for the three point function. The results here are actually less sensitive to the detailed fitting prescription than the fits to the two-point functions described in the last section. In Fig. 12 we show our data for the  $\rho\pi\pi$  three-point function with the pions at fixed time slices 0 and 4 as a function of the  $\rho$  time. The graphs include the reflected signal due to periodic boundary conditions. The solid line is the analytic evaluation of Eq. 3.12. Its shape agrees very well with our data. Our value of  $g_{\rho\pi\pi}$  comes from comparing the normalization of the two curves at the trough, where the  $\rho$  is farthest from the two pions; it is nice to see that about the same value for  $g_{\rho\pi\pi}$  is obtained even when the  $\rho$  is quite close to the pions. Values of energies, renormalization constants and  $g_{\rho\pi\pi}$  as function of the hopping constant  $K$  are shown in Table III. We have also included, for reference, values of the renormalized quark mass,  $(2K_c)^{-1} - (2K)^{-1}$ , where  $K_c$  is the critical  $K$  at which the pion mass is zero.

Table III strongly suggests that an extrapolation of  $g_{\rho\pi\pi}$  to the physical value of  $K$  can be done reliably. However, we note that while linearity of the three-point function in the strength  $\alpha$  of the external field was true to high accuracy on each lattice individually, the linear

extrapolation in  $1/K$  is good only statistically. Although linearity in  $1/K$  is excellent on the data analyzed as a whole, it is possible to find subsets of lattices for which  $g_{\rho\pi\pi}$  is not very linear as a function of  $1/K$ . For baryons the problem is somewhat worse than it is for mesons.

To test the consistency of our procedure, we evaluated the  $\rho\pi\pi$  three point function, which must be zero by  $g$ -parity conservation. We found it to be an order of magnitude smaller than the  $\rho\pi\pi$  three-point function, fluctuating in sign, and statistically consistent with zero.

Extensive checking was done to determine the extent to which excited states contaminated our results. It can be seen in Figure 12 that the raw data for the  $\rho\pi\pi$  three point function differs from the expected convolution of pure exponentials only by about 50%, even when the  $\rho$  operator is placed on the same time slice as one of the  $\pi$  operators. This is to be contrasted with the analogous results for the two point functions, which deviate from pure exponential form by over an order of magnitude when both operators are on the same time slice. Since our results are obtained by taking the  $\rho$  operator as far as possible from the two pions, it is clear without doing further checking that there is not likely to be significant contamination in our results due to excited  $\rho$  states. On the other hand, a  $\rho\pi\pi'$  signal has a shape very similar to the one we are looking for. We therefore repeated the entire calculation on three of our lattices using a different operator for the external  $\pi$  source, which connects to excited  $\pi$  states with a different ratio of renormalization constants. The operator we used was the nonlocal quark-antiquark operator at nearest neighbor sites connected by a link matrix. The behavior of the renormalization constants for operators of this type is shown in Figure 13 for various

separations. By examining the two point functions for these operators, we determined the ratio of the renormalization constants connecting the local and nonlocal operators to the pion state. Then, three-point function data using the nonlocal operators was analyzed using the  $Z$ 's for the nonlocal operators. The value of  $g_{\rho\pi\pi}$  for each of the three lattices was the same obtained with the local operator to an accuracy of 4%, indicating surprisingly little contamination from excited pion states. (see Table IV).

The statistical error estimates were again obtained by the method, described in the appendix, of performing the full analysis leading to the coupling constants on data sets with one or a few elements removed. Correlations between successive lattices may be tested for by comparing error estimates obtained by removing increasing numbers of consecutive lattices from the data set. For example, for the  $\Delta N\pi$  coupling constant at  $K=.355$ , for which we did a very extensive analysis, we obtained the value  $g=4.38\pm 0.93$ . The error estimates obtained for  $m=1,2,3,4,6$ , and 8 lattices removed were .66, .80, .89, .94, .93, and .89. The error estimate for this quantity does not level off until the bin size  $m=3$  ( $\approx 1500$  sweeps). This is in marked contrast to the errors on the hadron masses which were essentially constant for all bin sizes. We have averaged over all possible ways of removing  $m$  consecutive lattices from the data set, even though not all the ways are statistically independent. The error estimates for  $m$  larger than about 5 are not very reliable, since the number of independent subsamples becomes relatively small ( $\leq 4$ ). The accuracy of the errors themselves may be estimated by doing a second order jackknife, that is, doing a full jackknife on the data sets with a few lattices already removed. This is a lot of work and

we have done it only for the  $\Delta N\pi$  coupling constant at  $K=.355$ . The result is  $g=4.38\pm(0.93\pm 0.26)$ . For most of the coupling constants calculated, we saw correlations similar to those described above, lasting over 2 or 3 consecutive lattices. The statistical errors given in the fifth row of Table V are for a bin size  $m=4$ , which seemed to be the best compromise between removing the effects of correlations while keeping the largest possible number of independent subsamples ( $n/m=5$  in this case).

It is interesting to note that the statistical errors on  $g_{\rho\pi\pi}$ , shown in Table III are much smaller than some of the errors in the renormalization constants  $Z_\pi$  and  $Z_\rho$ , even though the expression for  $g_{\rho\pi\pi}$  is given in terms of the  $Z$ 's and the masses. This is because errors in the  $Z$ 's are very highly correlated with errors in the masses. When each propagator  $\sqrt{Z} e^{-mt}$  is truncated from the three-point function to obtain the coupling constant, errors in the two quantities cancel out rather well to leave a relatively small statistical error in  $g_{\rho\pi\pi}$ . The same effect makes  $g_{\rho\pi\pi}$  rather insensitive to the question of whether or not our lattice is long enough in time to see the pure particle pole. On the basis of the data 2 time slices away from the end of the lattice, we obtained somewhat higher masses as discussed in the preceding section, and much larger renormalization constants; on the other hand, the value of  $g_{\rho\pi\pi}$  obtained was almost unchanged.

Figure 14 is the graph of a typical baryon decay three point function, the  $\Delta N\pi$  amplitude. The local proton operator is at timeslice 0. The pion carries momentum, and is fixed at  $t=4$  as before. The amplitude is shown as a function of the timeslice of the  $\Delta$ , which is at rest. The data follow the theoretical expectation reasonably well, but

the agreement is not as spectacular as for the meson decay amplitudes. In particular, the fall-off of the three point function when the  $\Delta$  is far from the  $\pi N$  system has a different slope than that expected from the  $\Delta$  mass parameter obtained from analysis of the  $\Delta$  two point function. As may be seen from the figure, the value of the coupling constant obtained by matching the curve with the data will depend on the timeslice at which the data is fit. This introduces a source of error into the baryon coupling constants, possibly as large as 50%. For the meson decays, this was a negligible source of error. One possible explanation of this slope mismatch is that the lattice is not long enough in the time direction to project out the lowest mass state in the baryon two point function. If the three point function is less contaminated with excited states, as seemed to be the case for the mesons, it would give a truer (lighter) value for the baryon mass. We suspect that the greater difficulty of seeing the pure lowest mass baryon states is a contributing factor to the too large ratio of baryon to meson masses in many calculations of this type, including ours.

Table V contains our results at the three values of the light quark mass and the extrapolations to the proper light quark limit. The meson amplitudes are about a factor of  $1\frac{1}{2}$  to 2 below experiment, the baryon amplitudes a factor of 2 to  $2\frac{1}{2}$ . The additional discrepancy for baryons is in the right direction to have been caused by the slope mismatch noted above. The discrepancies with experiment are not uniform for the four decuplet baryon decays, meaning that width ratios as well as widths do not come out perfectly in our data. In fact, our width ratios are similar to those predicted by flavor SU(3) symmetry. The two sets of predictions are compared in Table VI.

There are at least two possible sources of error which might produce the factor of two discrepancy between our amplitudes and the experimental data. One is that our calculation has been done with one of the pions somewhat off mass shell ( $E^2 - q^2 - M^2 = -.29 \text{ GeV}^2$  for the  $\rho\pi\pi$  case); our results may thus be suppressed by a form factor. A crude estimate based on data for the process  $\pi\rho \rightarrow \rho\rho$  and the one-pion exchange model indicates that this effect may be rather large. Another potentially large source of error is the finite size of the lattice spacing. Strong coupling results for this amplitude yield  $g_{\rho\pi\pi} = 1.36$  and  $.98$ ,<sup>14</sup> a factor a 5 or 6 discrepancy with data. It would not be surprising if a discrepancy such as the one we find is obtained in the crossover region due to finite lattice spacing effects.

We should also mention errors due to the valence approximation and finite volume effects. We hope that these are not at the factor of two level, but we have no evidence one way or the other. The expectation value of the Wilson line on our lattices is roughly .03.

## VII. Conclusions

The most important result of our calculation is the demonstration that the investigation of multihadron processes in lattice gauge theory can be carried out on existing computers using reasonable amounts of computer time. The physics results we have obtained are qualitatively very reasonable. If the major source of the discrepancy with experiment is a form factor effect, substantial quantitative improvement should be possible by increasing the transverse dimension of the lattice by about a factor of two to bring the momentum of the decay down to near its physical value for the various decay processes. If, as is equally plausible, finite lattice spacing effects are very important, quantitative improvement may be more difficult. Many other processes can clearly be calculated using similar techniques, for example, electromagnetic form factors and decays of hadrons. This approach is now being used<sup>6</sup> to calculate weak matrix elements for the  $\Delta I=1/2$  rule.

## APPENDIX

In this Appendix we discuss our procedure for estimating statistical errors by subensemble analysis. Calculation of statistical errors in lattice gauge theory is complicated by the fact that consecutive lattices in an ensemble are not usually completely statistically independent. The correlation length depends on both the coupling constant and on the quantity being measured. This means that the standard formula for the estimated error

$$E^2 = \langle (x - \bar{x})^2 \rangle / (N-1) \quad (\text{A.1a})$$

cannot be applied naively. Wilson<sup>9</sup> has described how to deal with this problem for the case of Wilson loops. Eq. (A.1a) is generalized to

$$E^2 = \langle (x_m - \bar{x})^2 \rangle / (n/m-1) \quad (\text{A.1b})$$

where  $x_m$  is one of the set of averaged  $m$ -tuples of the set of  $x$ :  $(x_1 + \dots + x_m) / m$ . (A.1a) and (A.1b) are exactly equivalent when the average over all possible  $m$ -tuples is taken. They are equal in the mean when some random subset of subensembles is taken. When there are correlations between nearby lattices and the average is taken over the set of  $n/m$  subensembles of  $m$  consecutive lattices, (A.1b) gives a larger and truer estimate of the expected error. Since correlations tend to die out after enough iterations, as  $m$  is increased from one to 2, 4, 8, 16..., the expected error given by (A.1b) typically rises with each increase in  $m$  by a factor of about  $\sqrt{2}$  at first, and then levels off to the correct value.

For physical quantities such as hadron masses or the string tension it is impossible to apply this procedure unless the ensemble of lattices is huge. The basic problem is that these quantities involve taking a logarithm of a hadron propagator or of a function of Wilson loops. The loops or propagators are often negative on a few of the lattices in the ensemble, making it impossible to subensemble on groups as small as one or two configurations. Even with slightly larger subensembles, the physical quantities obtained from the subensembles are subject to wild fluctuations which do not necessarily average out, since taking the logarithm does not commute with the averaging operation.

In this appendix, we give a method for subensembling physical quantities which is stable and well behaved even for relatively small data sets. For large data sets, it gives estimated errors approximately equal to the standard subensembling procedure. For Wilson loops and similar quantities it is identical to the procedure used by Wilson. Our method is based on the jackknife procedure.<sup>15</sup> The fundamental jackknife formula is

$$E^2 = (n-1)\langle(\rho - \bar{\rho})^2\rangle \quad (\text{A.2a})$$

where  $\bar{\rho}$  is the result of an analysis of  $n$  data elements, and  $\rho$  is one of the results of an analysis on the  $n$  data sets of  $n-1$  elements each obtained by removing one of the elements of the original data set. If the analysis to be performed is simply the averaging of a set of numbers, then (A.2a) and (A.1a) are identical. However, for obtaining a mass from a set of  $n$  hadron propagators, (A.2a) gives a much more stable and accurate error estimate than would be obtained from the mean square of the masses obtained by analyzing individual propagators. In

addition, a simple extension of this formula permits accurate subensembling. The formula

$$\epsilon^2 = (n/m - 1) \langle (\rho_m - \bar{\rho})^2 \rangle, \quad (\text{A.2b})$$

where  $\rho_m$  is one of the results obtained from a data set with  $m$  elements removed, is also identical to its counterpart (A.1b) for the case of averaging a set of numbers. However, for hadron properties, the results  $\rho_m$  obtained from data sets with  $m = 1, 2,$  or  $4$  elements removed from the full ensemble of lattices are much more stable and reliable than the results obtained by analyzing a set of  $1, 2,$  or  $4$  lattices. When  $m$  is increased by a factor of two,  $\epsilon$  rises by roughly a factor of  $\sqrt{2}$  if the consecutive sets of lattices removed are highly correlated and stays roughly constant if they are uncorrelated. This method shares the problem of the ordinary subensembling procedure that the reliability of the error estimates decreases as the number of independent subensembles  $n/m$  becomes small.

We have emphasized the advantages of this method particular to lattice gauge theory calculations. We should also mention that this method and other related computer-intensive methods which are described in Ref. 15 have other advantages, in particular the possibility of relaxing the assumption of a normal distribution. It is also possible to calculate the reliability of the errors themselves by performing a second order jackknife to estimate the variance of the error estimate.

As reported above, we have applied this method very successfully to hadron masses and coupling constants. For most coupling constants, we found clear evidence for correlations which last up to 1000-1500 gauge sweeps ( $m=2$  or  $3$  in Eq. (A.2b)) and no evidence for correlations

thereafter. For masses, we found no evidence for correlations between lattices separated by 500 sweeps. The method required the complete automation of the analysis process in a computer program, but resulted in an understanding of statistical errors comparable to that obtainable for Wilson loops with a similar number of lattices.

References

†Address after Aug., 1985: Dept. of Physics, Indiana University, Bloomington, IN 47405

\*Work supported by the U.S. Department of Energy under Grant No. DE-AC02-76ER02220.

1. D. Weingarten, Phys. Lett. 109B, 57 (1982); Nucl. Phys. B215 [FS7], 1 (1983).
2. H. Hamber and G. Parisi, Phys. Rev. Lett. 47, 1792 (1981); E. Marinari, G. Parisi and C. Rebbi, Phys. Rev. Lett. 47, 1975 (1981).
3. C. Bernard, T. Draper and K. Olynyk, Phys. Rev. D27, 227 (1982); R. Gupta and A. Patel, Phys. Lett. 124B, 94 (1983); K. Bowler, G. Pawley, D. Wallace, E. Marinari and F. Rapuano, Nucl. Phys. B220 [FS8], 137 (1983); H. Lipps, G. Martinelli, R. Petronzio and F. Rapuano, Phys. Lett. 126B, 250 (1983); A. Hasenfratz, P. Hasenfratz, Z. Kunszt and C. B. Lang, Phys. Lett. 110B, 289 (1982); J. P. Gilchrist, H. Schneider, G. Schierholz, and M. Teper, Phys. Lett. 136B, 87 (1984).
4. C. Bernard, T. Draper, K. Olynyk and M. Rushton, Phys. Rev. Lett. 49, 1076 (1982); G. Martinelli, G. Parisi, R. Petronzio and F. Rapuano, Phys. Lett. 116B, 434 (1982).
5. R. C. Brower, M. B. Gavela, R. Gupta, and G. Maturana, Phys. Rev. Lett. 53, 1318 (1984); N. Cabibbo, G. Martinelli, and R. Petronzio, Nuc. Phys. B244, 381, (1984).

6. C. Bernard, in Gauge Theory on a Lattice: 1984, Argonne National Laboratory Workshop.
7. J. Kogut, M. Stone, H. Wyld, W. Gibbs, J. Shigemitsu, S. Shenker, D. Sinclair, Phys. Rev. Lett. 50, 393 (1983); I. Barbour, P. Gibbs, J. Gilchrist, H. Schneider, M. Teper, Phys. Lett. 136B, 80 (1984).
8. S. Gottlieb, P. Mackenzie, H. Thacker and D. Weingarten, Phys. Lett. 134B, 346 (1984); S. Gottlieb in Gauge Theory on a Lattice: 1984, Argonne National Laboratory, ed. by C. Zachos, W. Celmaster, E. Kovacs, and D. Sivers.
9. M. Creutz, L. Jacobs and C. Rebbi, Phys. Rev. Lett. 42, 1390 (1979); K. Wilson, in Recent Developments in Gauge Theories (Cargese, 1979), ed. G. 't Hooft et al., Plenum (1980).
10. D. Weingarten and D. Petcher, Phys. Lett. 99B, 333 (1981).
11. W. Duffy, G. Guralnik and D. Weingarten, Phys. Lett. 125B, 311 (1983).
12. K. C. Bowler, D. L. Chalmers, A. Kenway, R. D. Kenway, G. S. Pawley and D. J. Wallace, Nuc. Phys. B240, 213 (1984).
13. H. Lipps, G. Martinelli, R. Petronzio and F. Rapuano, Phys. Lett. 126B, 250 (1983).
14. N. Vasanti, Nuc. Phys. B118, 533 (1977). J. Smit, private communication.  $\rho$  decay has also been calculated using the SLAC fermion approach by B.F.L. Ward, Phys. Rev. D25, 1330 (1982).

15. For a review see B. Efron, SIAM Review 21, 460 (1979) and references therein.

TABLE I

Variation of masses due to fitting procedure. Masses are extrapolated to the chiral limit. The first column (DE) contains masses obtained from a double exponential fit. The last three columns (EM) are the effective masses at timeslices 6, 7 and 8 respectively.

	DE	EM 6	EM 7	EM 8
	Mass (lattice units)			
$\rho$	0.545	0.738	0.610	0.558
N	0.999	1.131	1.042	0.952
$\Delta$	1.357	1.492	1.381	1.394
K	0.671	0.716	0.670	0.671
$K^*$	0.797	0.934	0.823	0.799
$\Sigma$	1.235	1.407	1.300	1.194
$\Sigma^*$	1.522	1.667	1.553	1.555
$\Xi$	1.440	1.612	1.464	1.445
$\Xi^*$	.680	1.854	1.716	1.724
	Mass ratio $M/M_N$			
$\rho$	0.546	0.652	0.586	0.586
N	1.000	1.000	1.000	1.000
$\Delta$	1.358	1.318	1.327	1.464
K	0.671	0.632	0.643	0.705
$K^*$	0.798	0.825	0.790	0.839
$\Sigma$	1.236	1.243	1.247	1.254
$\Sigma^*$	1.523	1.472	1.490	1.634
$\Xi$	1.441	1.424	1.404	1.516
$\Xi^*$	1.681	1.638	1.646	1.810

**TABLE II**  
Comparison of masses with experiment

	Particle Mass (GeV)	
	Lattice	Experiment
N	.932 $\pm$ .092	.938
$\Delta$	1.232 (input)	1.232
$\Sigma$	1.155 $\pm$ .063	1.194
$\Lambda$	1.124 $\pm$ .068	1.115
$\Sigma^*$	1.377 $\pm$ .055	1.385
$\Xi$	1.327 $\pm$ .045	1.318
$\Xi^*$	1.523 $\pm$ .037	1.530
$\Omega^-$	1.672 (input)	1.672
$\pi$	.138 (input)	.138
$\rho$	.562 $\pm$ .072	.769
K	.605 $\pm$ .017	.495
$K^*$	.746 $\pm$ .042	.892

TABLE III

Energies, decay constants and  $g_{\rho\pi\pi}$  for three values of the hopping parameter  $K$ . The pions have momentum  $2\pi/12a \approx 520$  MeV.

$K$	$E_{\pi}$	$Z_{\pi}$	$M_{\rho}$	$Z_{\rho}$	$g_{\rho\pi\pi}$	$(2K)^{-1}$	$-(2K_c)^{-1}$
.325	1.14 $\pm$ .011	0.328 $\pm$ .018	1.12 $\pm$ .021	0.287 $\pm$ .025	2.76 $\pm$ .19	.248	
.340	1.01 $\pm$ .013	0.317 $\pm$ .024	0.996 $\pm$ .031	0.207 $\pm$ .031	2.84 $\pm$ .25	.180	
.355	0.882 $\pm$ .015	0.316 $\pm$ .031	0.877 $\pm$ .050	0.139 $\pm$ .036	3.01 $\pm$ .40	.118	

TABLE IV

Ratio of  $g_{\rho\pi\pi}$  from local and nonlocal pion operators.

	$g_{loc}/g_{nonloc}$	
	K = .325	K = .355
Lattice 2	1.03	1.05
Lattice 6	.93	.98
Lattice 9	.96	.98
Average	.97±.04	1.00±.03

TABLE V

Hadronic coupling constants compared with experiment

K	$\Delta \rightarrow N\pi$	$\Sigma^* \rightarrow \Sigma\pi$	$\Sigma^* \rightarrow \Lambda\pi$	$\Xi^* \rightarrow \Xi\pi$	$NN\pi$	$K^* \rightarrow K\pi$	$\rho \rightarrow \pi\pi$
.325	4.83	2.40	4.15	2.38	8.12	1.31	2.74
.34	4.79	2.44	4.22	2.48	7.94	1.53	2.78
.355	4.38	2.36	4.03	2.50	7.18	1.87	2.87
$K_C$	4.06 $\pm 1.09$	2.35 $\pm .62$	3.98 $\pm .83$	2.63 $\pm .53$	6.46 $\pm .67$	2.33 $\pm .38$	3.23 $\pm .61$
Expt.	11.10	4.96	9.04	5.23	13.4	3.26	6.11

TABLE VI

Comparison of width ratios with SU(3) predictions

	$\frac{\Gamma(\Sigma^* \rightarrow \Sigma \pi)}{\Gamma_{\Delta}}$	$\frac{\Gamma(\Sigma^* \rightarrow \Lambda \pi)}{\Gamma_{\Delta}}$	$\frac{\Gamma(\Sigma^* \rightarrow \Xi \pi)}{\Gamma_{\Delta}}$
Experiment	.036	.267	.079
SU(3) Symmetry	.056	.356	.165
Monte Carlo	.067	.374	.166

## FIGURE CAPTIONS

- Fig. 1: Schematic graphs of quark contributions to meson two-point functions in the quenched approximation (Fig. 1a) and the full theory (Fig. 1b).
- Fig. 2: Pion propagator as a function of Euclidean time for the hopping parameter  $K=.355$ . The solid line is the two-exponential fit using Eq. (5.2); the dashed line is the contribution to the fit of the lighter state.
- Fig. 3: Same as Fig. 2, but for the  $\rho$  propagator.
- Fig. 4: "Effective masses" of the  $\pi$  (crosses) and  $\rho$  (circles) as a function of  $t$ , obtained from the propagator data of Figs. 2 and 3 via Eq. (5.3).
- Fig. 5:  $\Delta$  propagator as a function of Euclidean time for the hopping parameter  $K=.355$ . The solid line is the two-exponential fit using Eq. (5.4); the dashed line is the contribution to the fit of the lighter state.
- Fig. 6: Same as Fig. 5, but for the nucleon propagator.
- Fig. 7: "Effective masses" for the  $\Delta$  and nucleon as a function of  $t$ , obtained from the propagator data of Figs. 5 and 6 via Eq. (5.5).
- Fig. 8: Effective mass plot for the four spin states of the nucleon and antinucleon analyzed individually. The nucleon with spin up is represented by  $*$ , with spin down

by +. The antinucleon with spin up is represented by x, with spin down by o.  $K=.355$ .

Fig. 9: Effective mass plot for the four spin states of the  $\Delta$ , analyzed individually. The  $3/2$ ,  $1/2$ ,  $-1/2$ , and  $-3/2$  states are represented by \*, +, x, and o respectively.  $K=.355$ .

Fig. 10: Effective mass plot for subsets of the nucleon data at  $K=.355$ . There are four subsets of data containing lattices 1-5, 6-10, etc.

Fig. 11: The  $\rho$  mass (solid line) and the mass squared of the pion (dotted line) plotted vs. the inverse hopping parameter.

Fig. 12: Data for the  $\rho\pi\pi$  three-point function (crosses) as a function of the time slice of the  $\rho$ . The pions are fixed at time slices 0 and 4. The solid curve is the theoretical expectation based on Eq. (3.12) with parameters fixed by the two-point function results. It is normalized by fixing  $g_{\rho\pi\pi}$  so that the solid curve fits the Monte Carlo data where the  $\rho$  is far from the pions.

Fig. 13: Connection of various quark bilinear operators with the pion state. The quark and the antiquark operators are separated in a straight line a distance  $m$  lattice spacings.

Fig. 14: Data for the  $\Delta N_\pi$  three-point function as a function of the time slice of the  $\Delta$ . A pion with momentum is fixed at time slice 4, and a local proton operator is at site 0. The solid curve is the theoretical expectation.



Fig. 1a

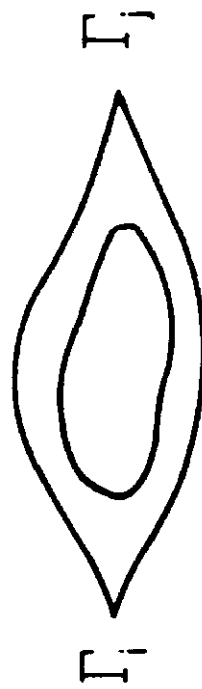


Fig. 1b

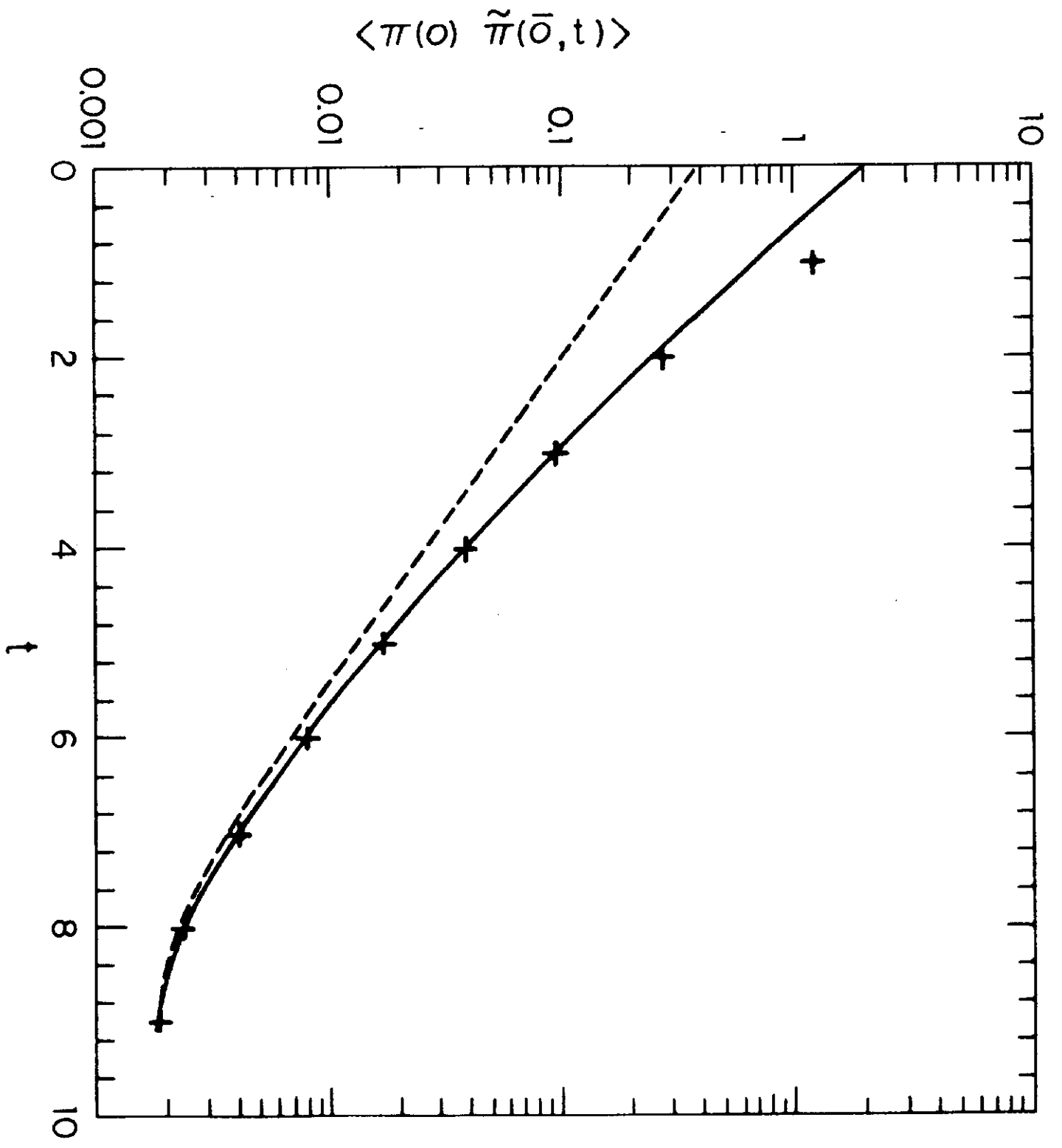


FIG. 2

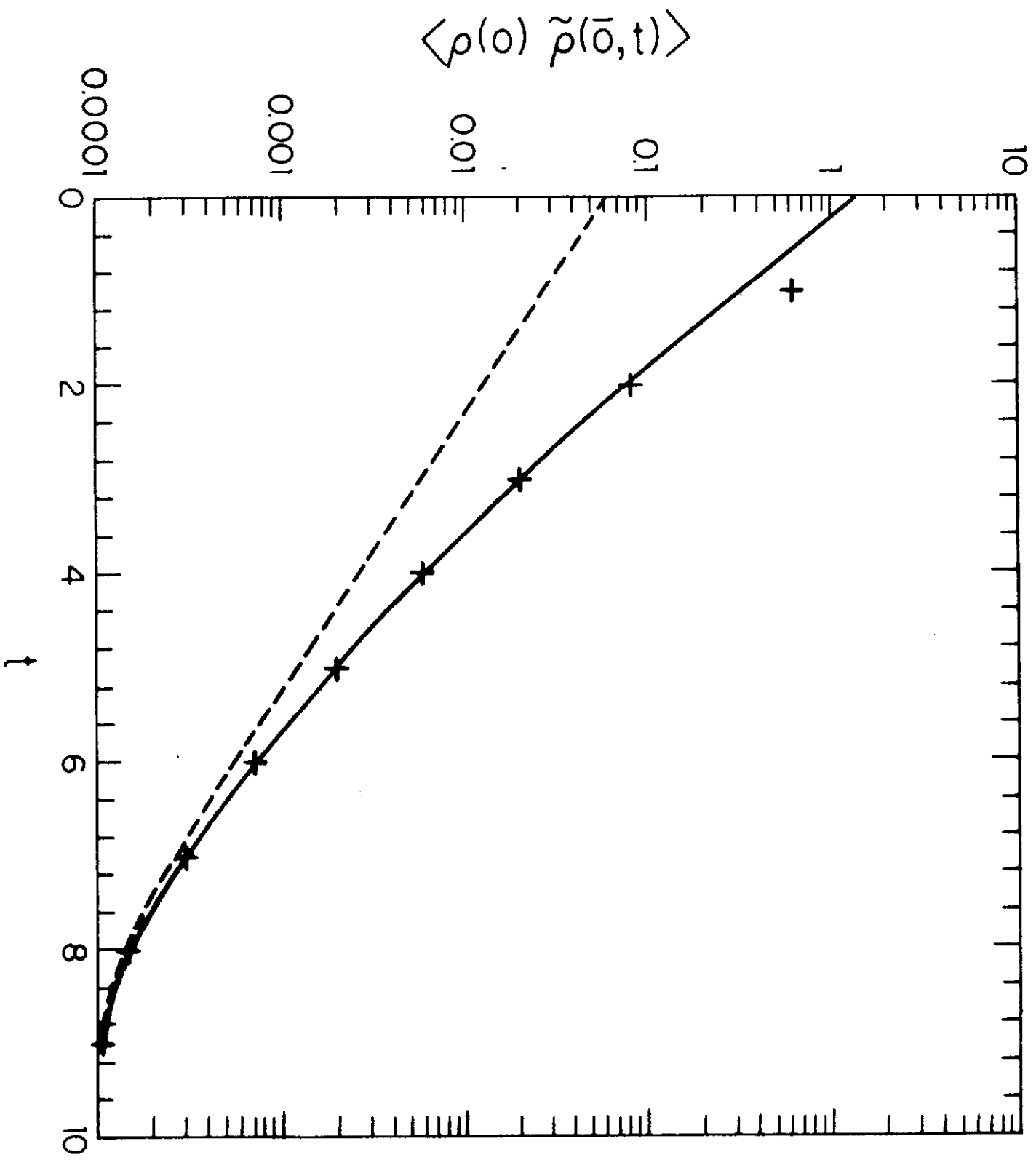


FIG. 3

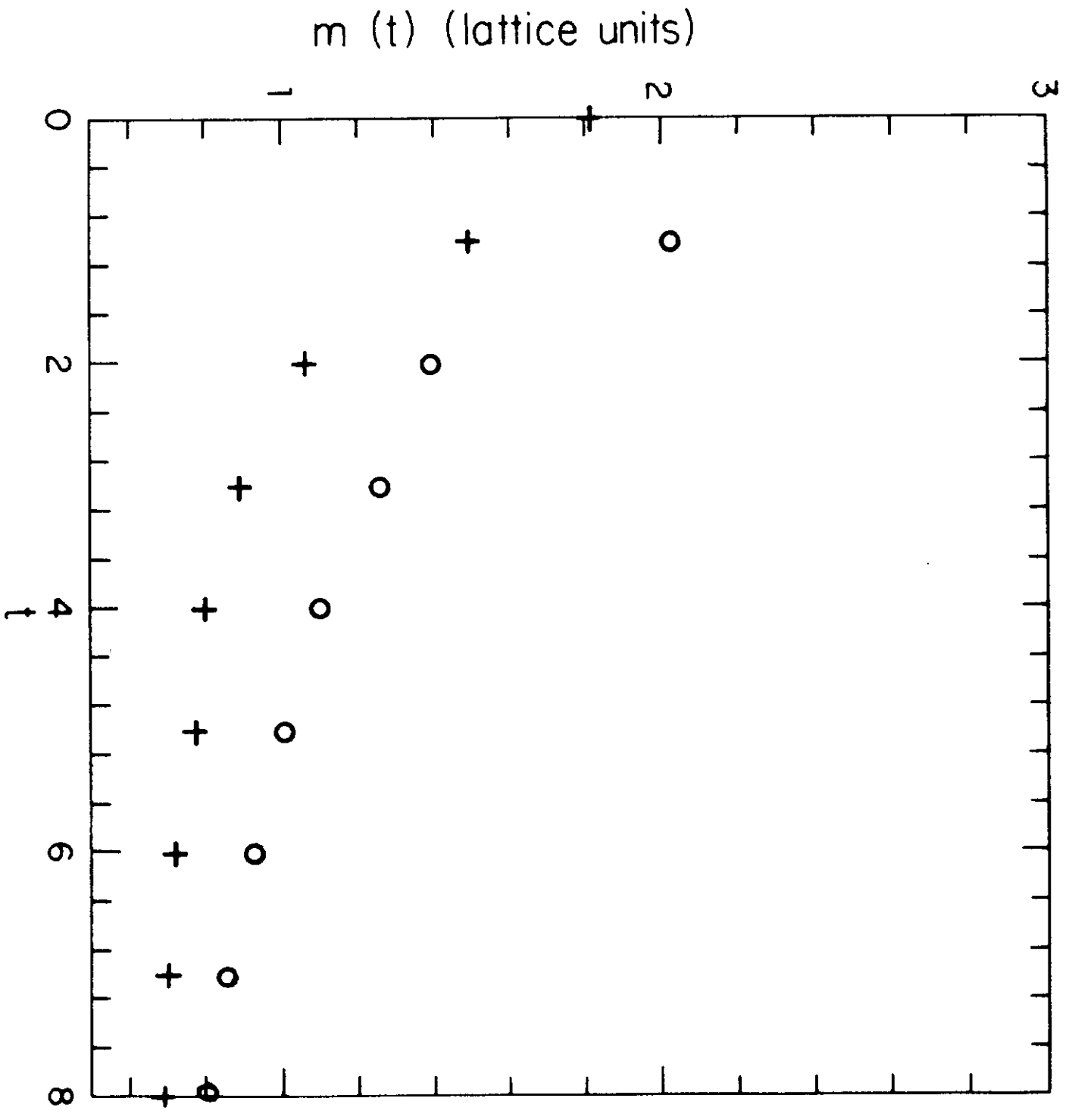


FIG. 4

$\langle \Delta^+(\circ) \tilde{\Delta}(\bar{\sigma}, t) \rangle$  (lattice units)

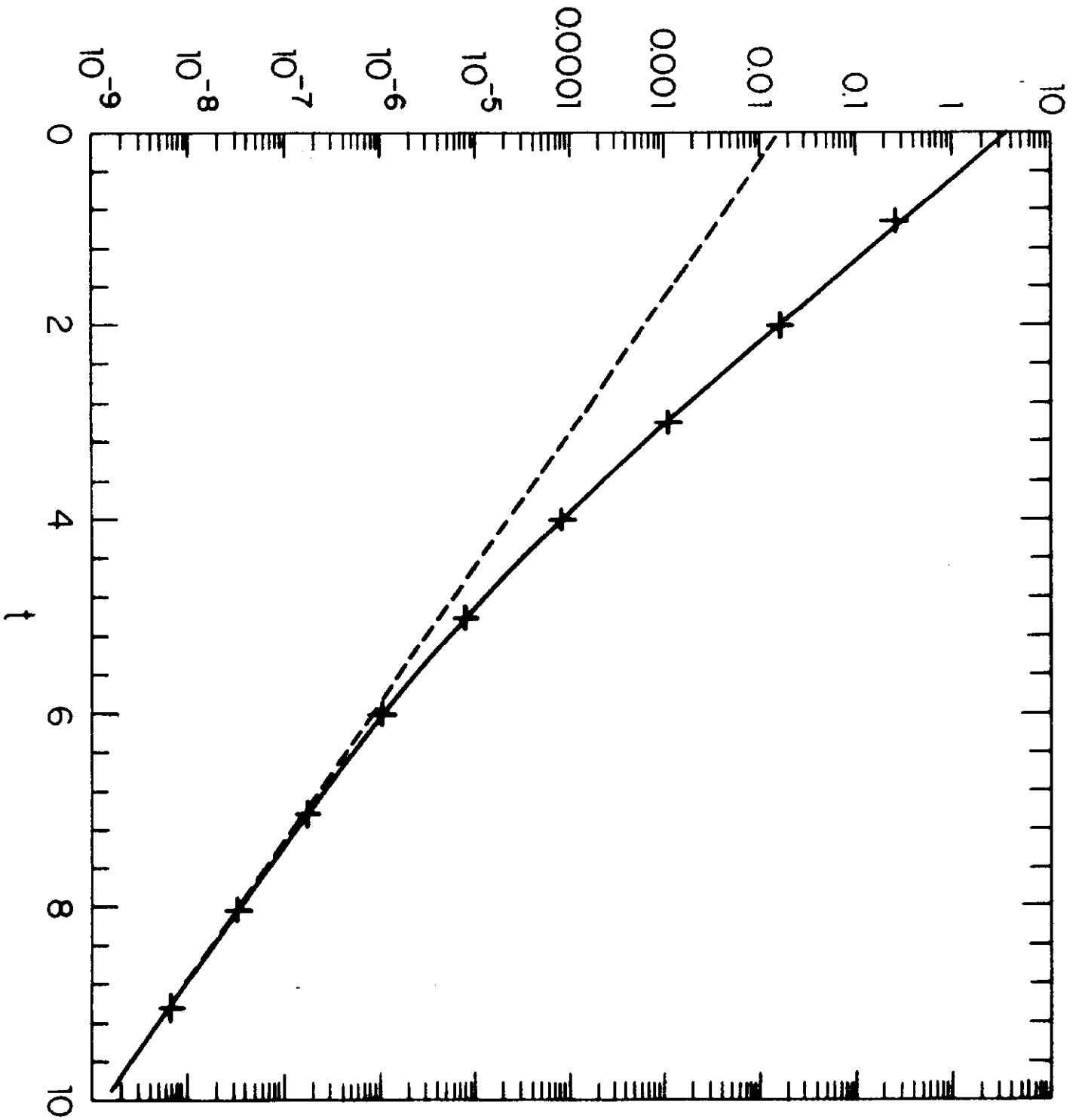


FIG. 5

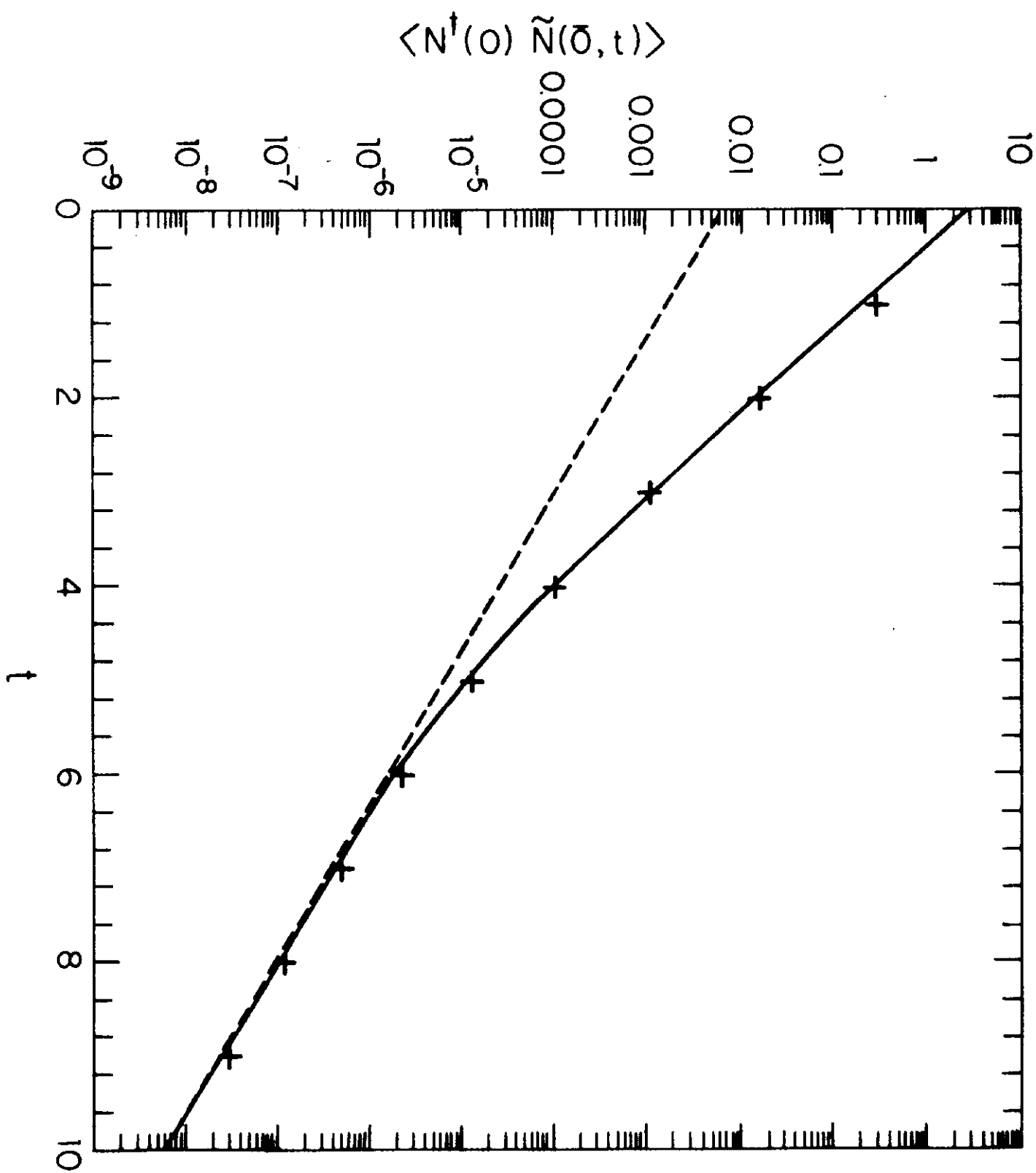


FIG. 6

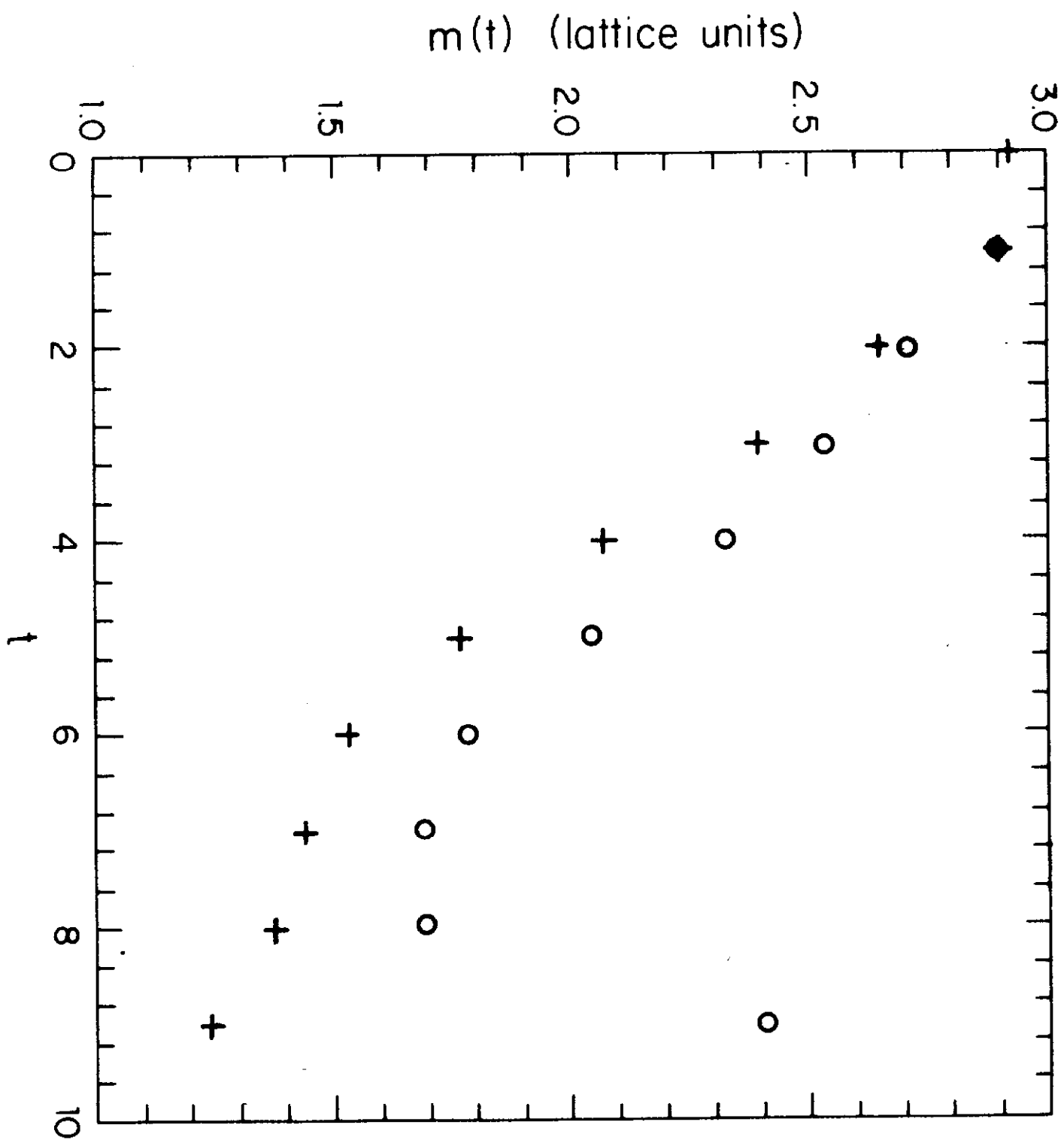


FIG. 7

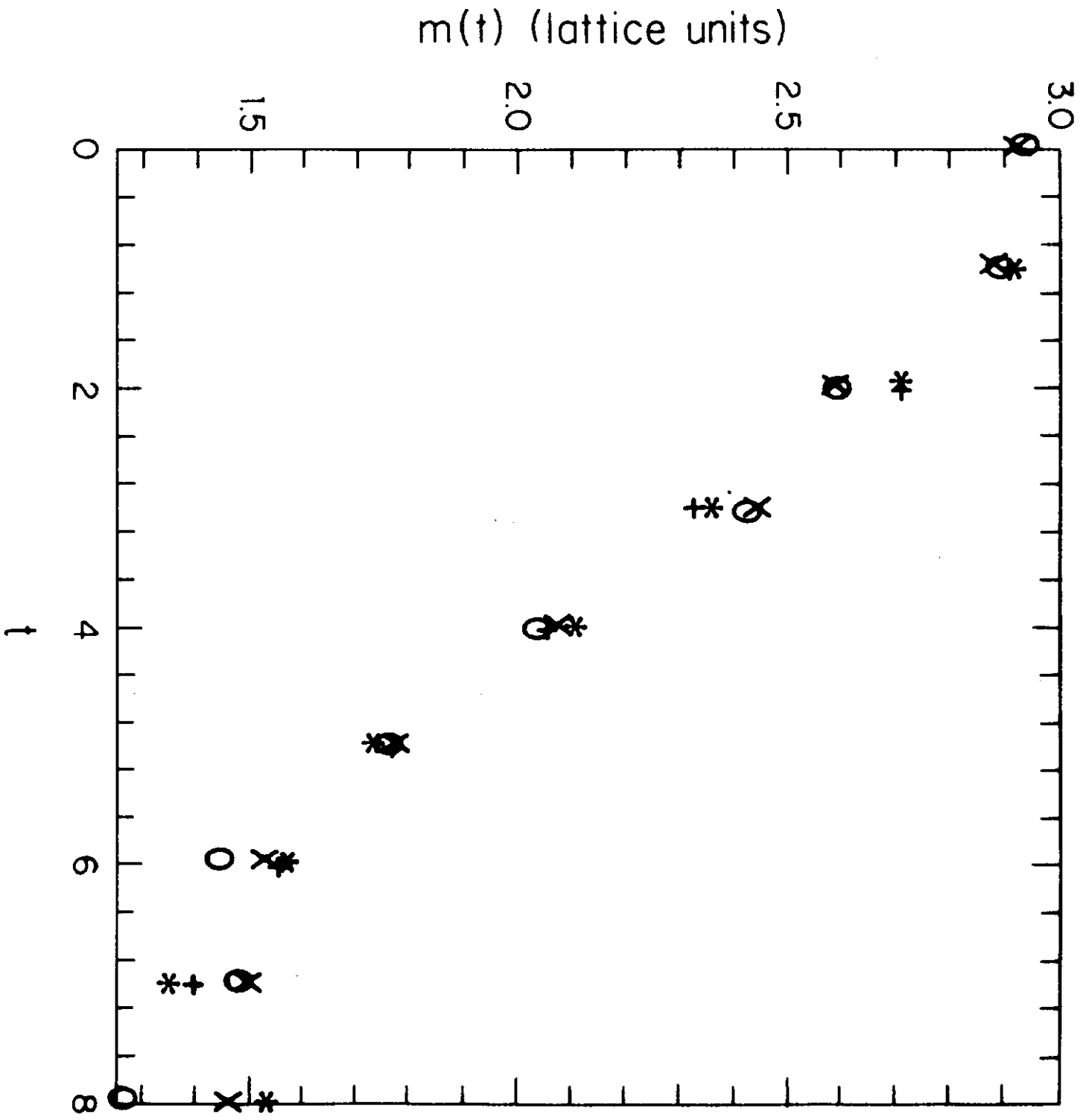


FIG. 8

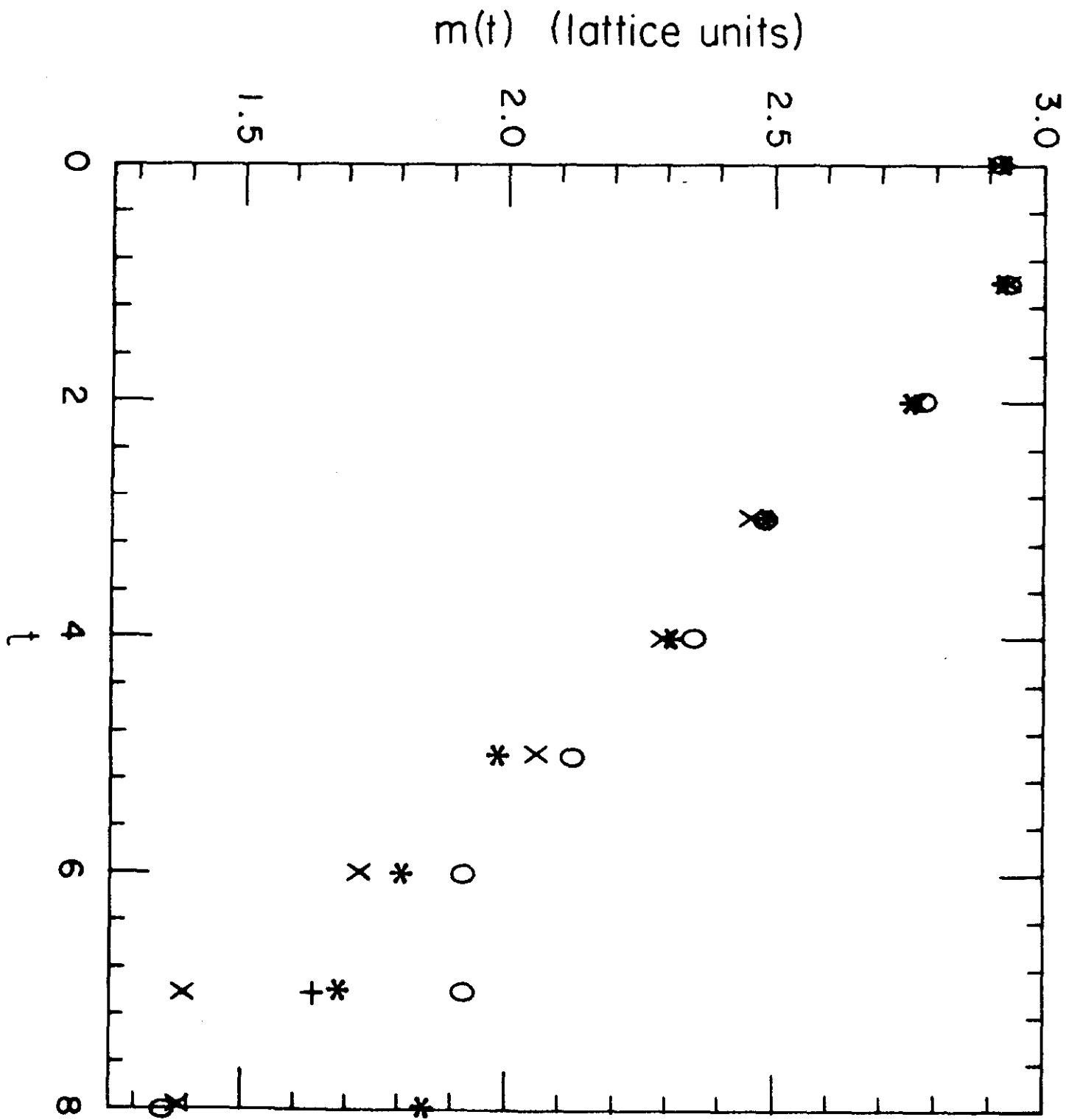


FIG. 9

$m(t)$  (lattice units)

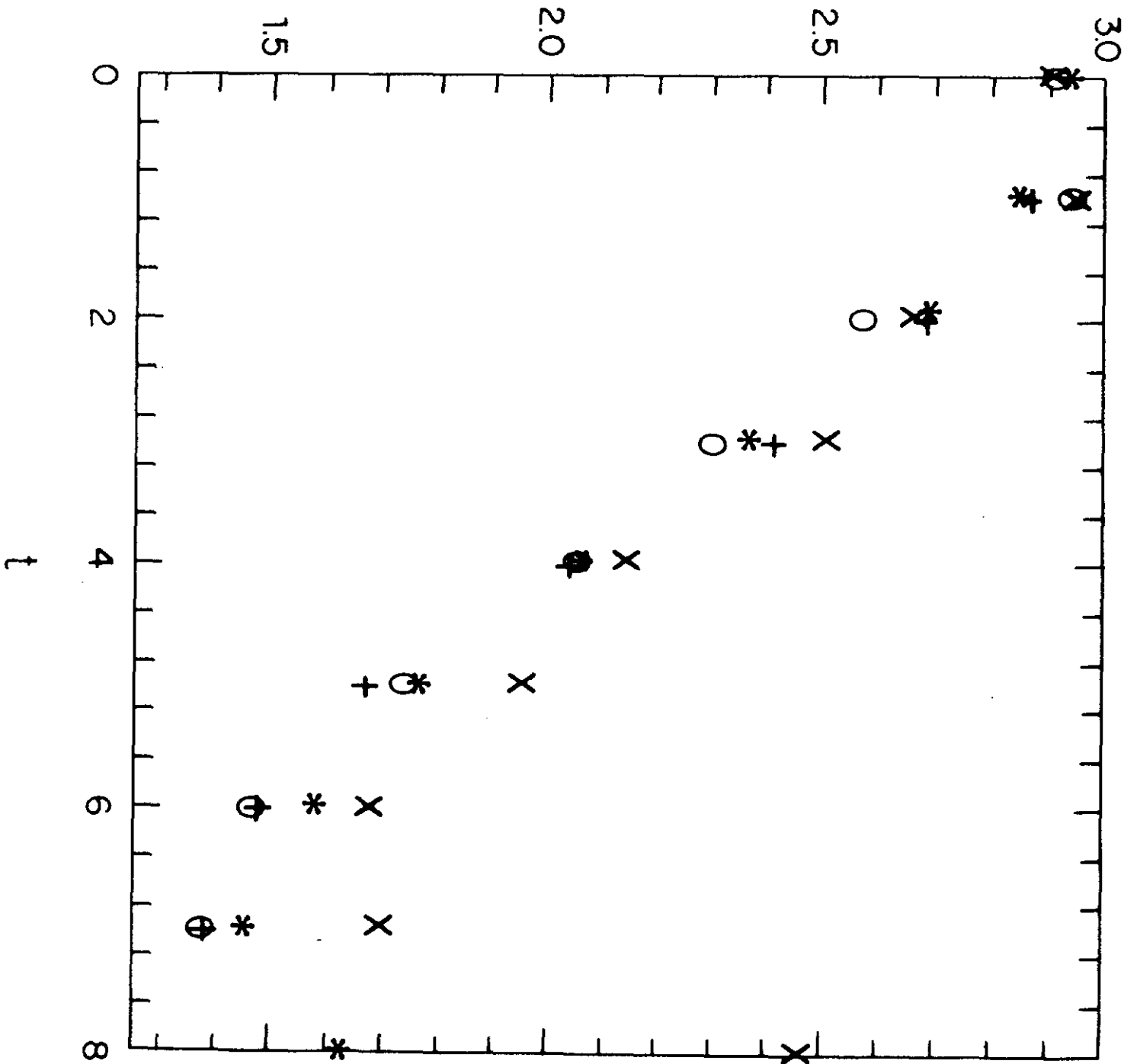


FIG. 10

$m_\rho$  and  $m_\pi^2$  (lattice units)

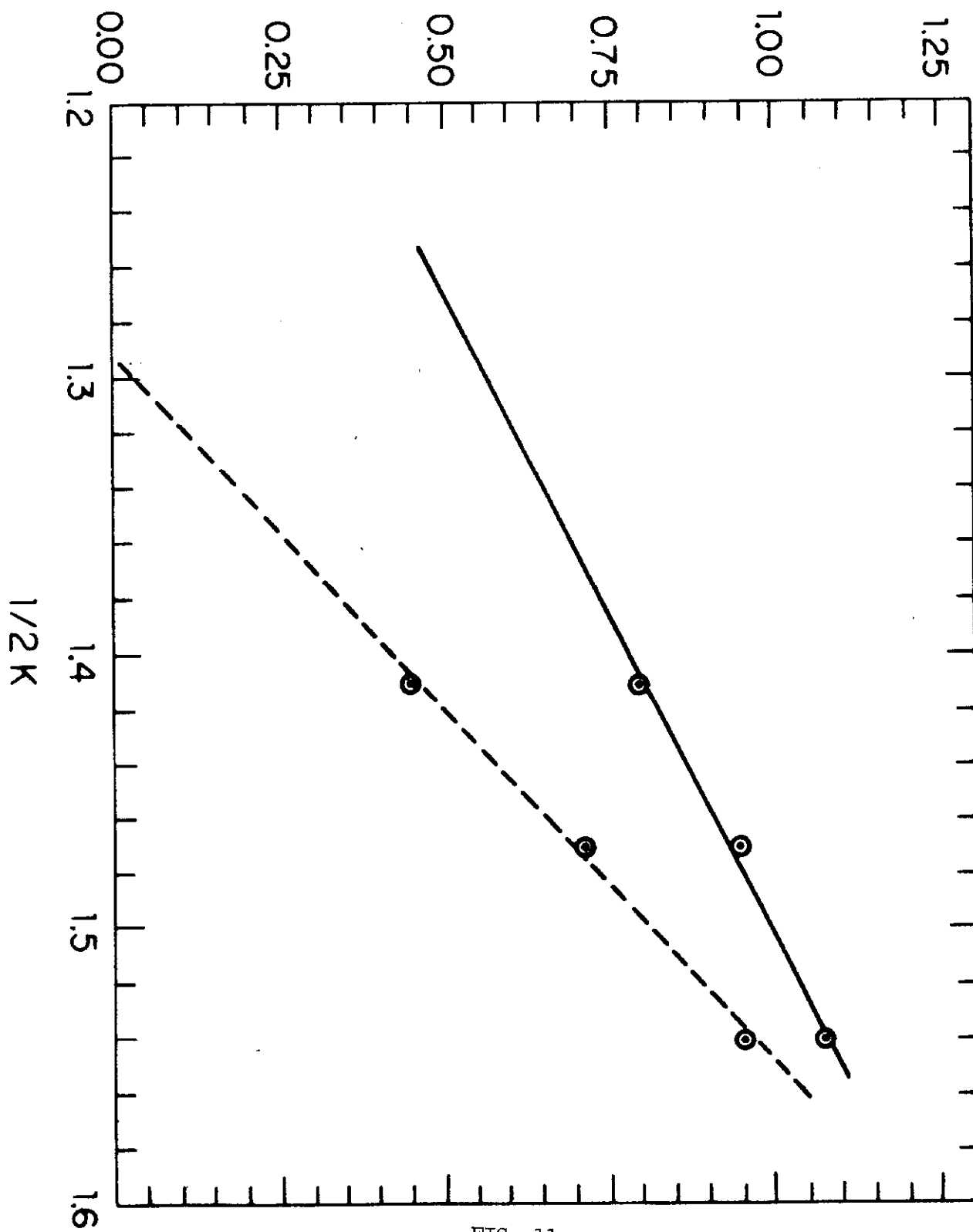


FIG. 11

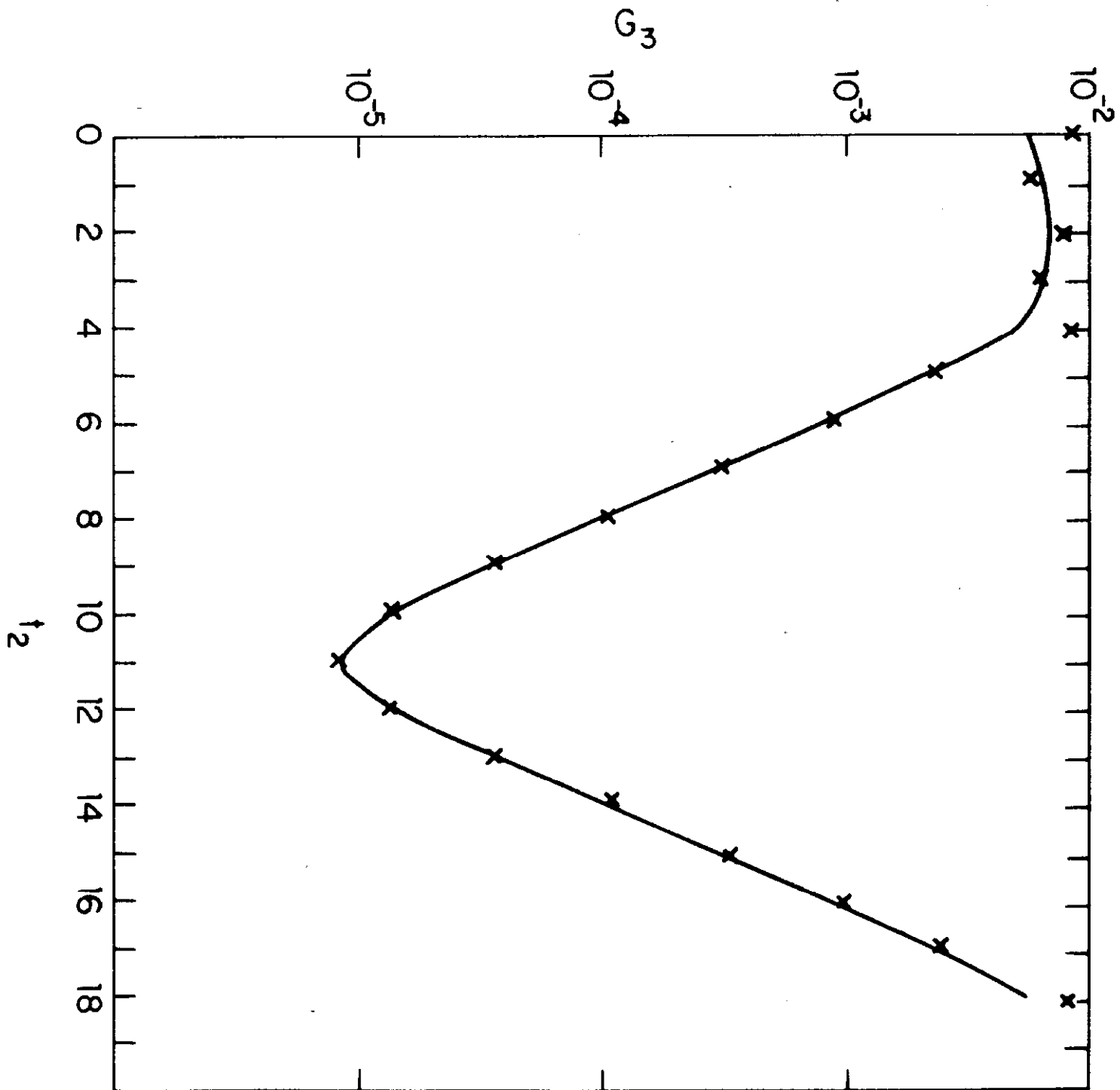


FIG. 12

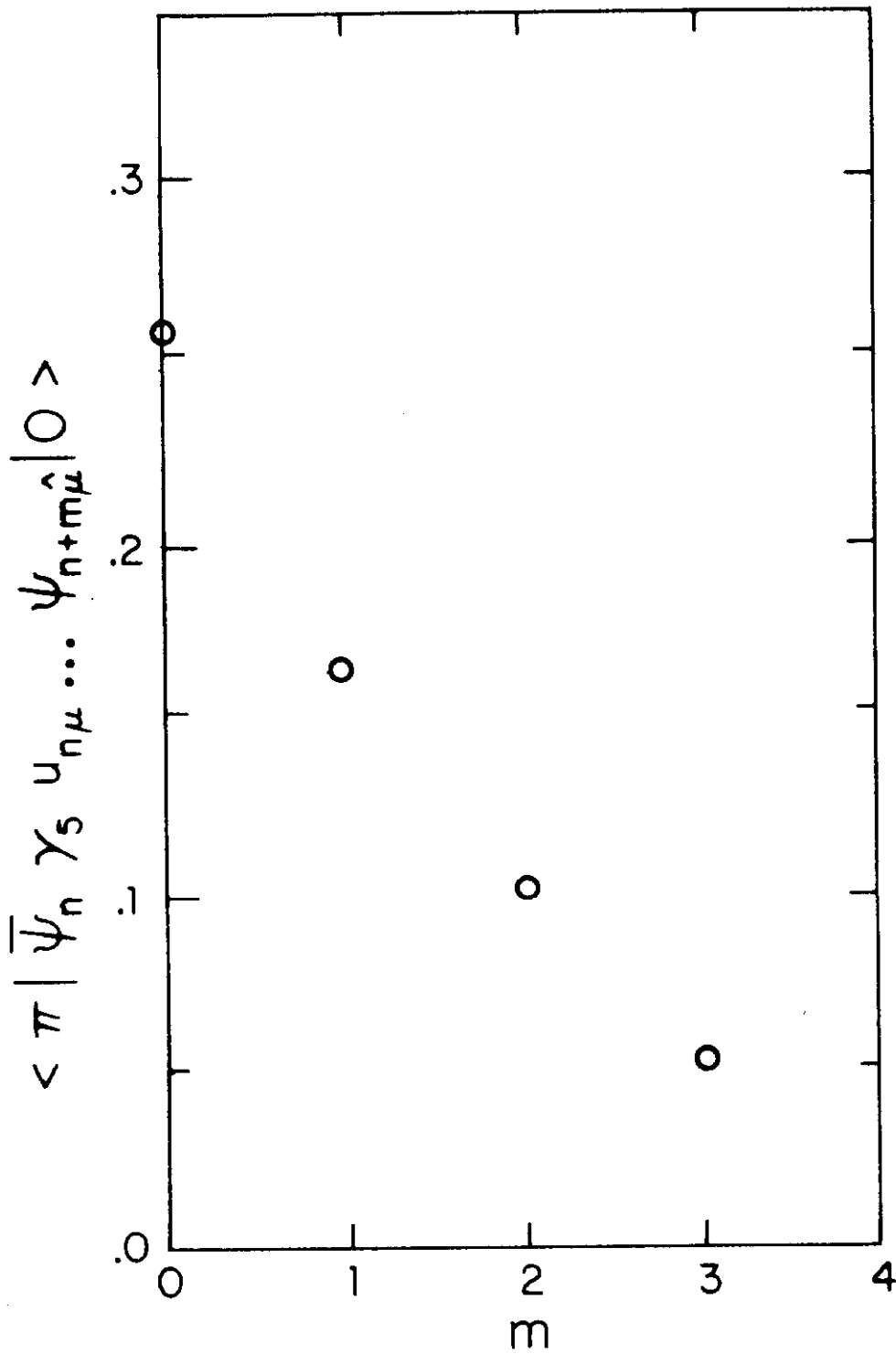


Fig. 13

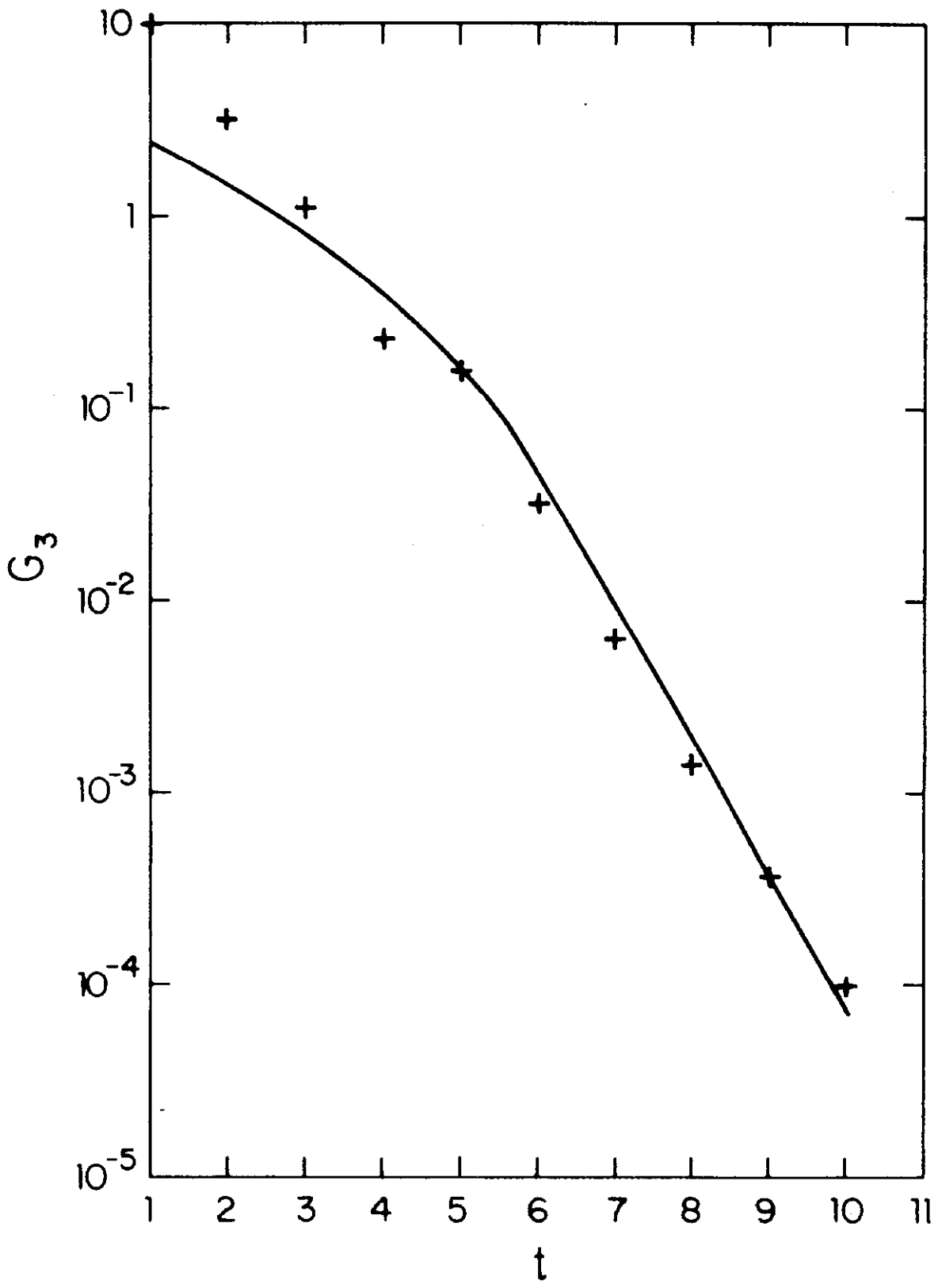


Fig. 14